



HAL
open science

Alkyl chain length influence of the functionalized diethanolamine ligand on the slow relaxation of the magnetization in $\text{CoIII}_3\text{DyIII}_3$ complexes

Chloë Bonnenfant, Nahir Vadra, Mathieu Rouzières, Rodolphe Clérac, Fabio D Cukiernik, Pablo Alborés

► **To cite this version:**

Chloë Bonnenfant, Nahir Vadra, Mathieu Rouzières, Rodolphe Clérac, Fabio D Cukiernik, et al.. Alkyl chain length influence of the functionalized diethanolamine ligand on the slow relaxation of the magnetization in $\text{CoIII}_3\text{DyIII}_3$ complexes. Dalton Transactions, 2024, 53 (6), pp.2815-2825. 10.1039/d3dt03656a . hal-04445243

HAL Id: hal-04445243

<https://hal.science/hal-04445243v1>

Submitted on 7 Feb 2024

HAL is a multi-disciplinary open access archive for the deposit and dissemination of scientific research documents, whether they are published or not. The documents may come from teaching and research institutions in France or abroad, or from public or private research centers.

L'archive ouverte pluridisciplinaire **HAL**, est destinée au dépôt et à la diffusion de documents scientifiques de niveau recherche, publiés ou non, émanant des établissements d'enseignement et de recherche français ou étrangers, des laboratoires publics ou privés.

Alkyl chain length influence of the functionalized diethanolamine ligand on the slow relaxation of the magnetization in $\{\text{Co}^{\text{III}}\text{Dy}^{\text{III}}\}$ complexes†

Chloë Bonnenfant,^{a,b} Nahir Vadra,^a Mathieu Rouzières,^c Rodolphe Clérac,^c Fabio D. Cukiernik^{*a} and Pablo Alborés^{*a}

We report the synthesis, structural characterization and magnetic properties of a series of Co(III)/Dy(III) complexes built up from an *N*-alkyl derivatized amino-alcohol ligand diethanolamine, functionalized with $\text{C}_n\text{H}_{2n+1}$ alkyl chains ($n = 3, 4, 6, 8$ and 10). While $n = 3$ afforded a butterfly $\{\text{Co}_2^{\text{III}}\text{Dy}_2^{\text{III}}\}$ core, the other alkyl chains ($n = 4, 6, 8$) afforded hexanuclear triangle-in-triangle $\{\text{Co}_3^{\text{III}}\text{Dy}_3^{\text{III}}\}$ complexes as shown by single-crystal X-ray determinations. Infrared spectroscopy allows us to characterize the C_{10} derivative complex, which did not crystallize. Magnetic ac susceptibility data collected below 10 K at driving frequencies up to 10 kHz under zero-dc field and up to 1 T provide insight into the SMM behaviour of the studied complexes. The characteristic time of the magnetization dynamics can be understood in terms of the competing Raman, Direct and Orbach-like mechanisms. A relationship between the magnetization dynamics within the family of complexes and the increasing alkyl chain length is discussed.

The characteristic time for magnetization reversal in molecular systems is the key feature of single-molecule magnet (SMM) behaviour.¹ Long relaxation times induced by a large energy barrier without quantum magnetization tunnelling relaxation are necessary for potential applications of these systems as data storage devices.² Lanthanide-based SMMs^{3–5} as well as heterometallic 3d/4f complexes⁶ have been prepared and studied for this purpose during the last two decades. Among the lanthanide series, Dy(III) SMMs are largely the most explored due to their strong axial magnetic anisotropy that can be engineered with a fine tuning of its coordination sphere.⁷ Indeed, the most promising SMMs up to now are based on Dy(III) ions.^{8–10}

Among heterometallic 3d/4f SMMs, the systems based on a Co(III)/4f metal combination are particularly attractive as the Co(III) ion is a closed shell center, hence leaving all magnetic features to the lanthanide ion. The Co(III) sites provide useful connectivity and

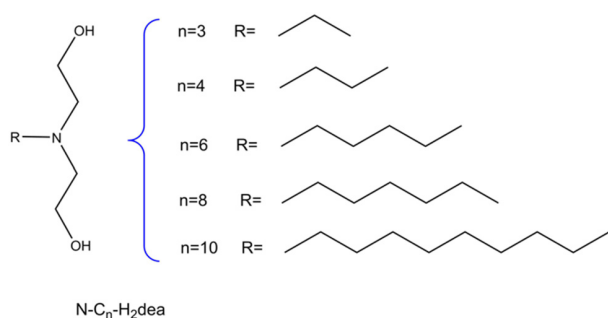
offer structural versatility in these heteronuclear complexes. Most of the studied examples in this category of SMMs are those showing a $\{\text{Co}_2^{\text{III}}\text{Dy}_2^{\text{III}}\}$ butterfly core, which is stabilized by chelating amino-alcohol-type ligands, such as triethanolamine or diethanolamine derivatives.^{11–18} In fact, some key magneto-structural correlations have been identified showing that small perturbations in the axial anisotropy of Dy(III) sites have a strong influence on the magnetization relaxation time.¹⁹

In order to test the structural modulation of the SMM properties in the Co(III)/Dy(III) system, we decided to take advantage of diethanolamine and the possibility to chemically functionalize this ligand at the N atom. Previous examples of Co(III)/Dy(III) complexes with *N*-methyl (*N*-methyldiethanolamine, H_2mdea) and *N*-butyl (*N*-butyldiethanolamine, H_2bdea) derivatives have been reported with most of them exhibiting the butterfly $\{\text{Co}_2^{\text{III}}\text{Dy}_2^{\text{III}}\}$ motif.^{12,14,17,18,20} In this work, we have prepared the $\text{N-C}_n\text{-H}_2\text{dea}$ ligands with $n = 3, 4, 6, 8$ and 10 (Scheme 1) and explored their reactions with the Co(II) pivalate precursor and Dy(III) nitrate. We found that a triangle-in-triangle $\{\text{Co}_3^{\text{III}}\text{Dy}_3^{\text{III}}\}$ core structure is obtained for the $n \geq 4$ ligands, affording complexes of formula $[\text{Co}_3^{\text{III}}\text{Dy}_3^{\text{III}}(\text{C}_n\text{-dea})_3(\text{piv})_7(\text{OH})_4(\text{H}_2\text{O})_2](\text{NO}_3)_n$, $n = 4$ (**1-C₄**) and $n = 8$ (**3-C₈**); and $[\text{Co}_3^{\text{III}}\text{Dy}_3^{\text{III}}(\text{C}_n\text{-dea})_3(\text{piv})_7(\text{OH})_4(\text{H}_2\text{O})(\text{NO}_3)]$, $n = 6$ (**2-C₆**) and $n = 10$ (**4-C₁₀**). The triangle-in-triangle $\{\text{Co}_3^{\text{III}}\text{Dy}_3^{\text{III}}\}$ motif was previously observed in two related complexes.^{20,21} Instead, the butterfly $[\text{Co}_2^{\text{III}}\text{Dy}_2^{\text{III}}(\text{C}_3\text{-dea})_3(\text{piv})_6(\text{OH})_2]$ (**5-C₃**) is obtained for $n = 3$, sharing the same molecular structure with the previously reported $[\text{Co}_2^{\text{III}}\text{Dy}_2^{\text{III}}(\text{mdea})_3(\text{piv})_6(\text{OH})_2]$,¹⁸ where the H_2mdea

^aDepartamento de Química Inorgánica, Analítica y Química Física/INQUIMAE (CONICET), Facultad de Ciencias Exactas y Naturales Universidad de Buenos Aires, Pabellón 2, Ciudad Universitaria, C1428EHA Buenos Aires, Argentina.
E-mail: albores@qi.fcen.uba.ar, fabioc@qi.fcen.uba.ar; Fax: +5411/4576-3341

^bOn leave from Ecole Européenne d'Ingénieurs de Chimie, Polymères et Matériaux, Université de Strasbourg, France

^cUniv. Bordeaux, CNRS, CRPP, UMR 5031, F-33600 Pessac, France



Scheme 1 Diethanolamine ligand derivatives (N-C_n-H₂dea) employed for the synthesis of the reported complexes.

ligand is N-C₁-H₂dea. Here, we are taking advantage of the $n = 4$ – 10 series of complexes preserving their {Co^{III}Dy^{III}} core, to study the influence that the alkyl chain length may exert over the structural organization and magnetization relaxation of these SMM complexes.

Synthesis and structural characterization

We have previously explored synthetic strategies to develop complexes that combine Co(III) and Ln(III) ions by employing amino-alcohol-type ligands like triethanolamine (H₃tea) and *N*-methyldiethanolamine (H₂mdea).^{16,18} The reaction of Co(II) pivalate precursor with lanthanide(III) nitrate in the presence of these ligands in acetonitrile afforded butterfly-like complexes with {Co(III)₂Dy(III)₂} metallic cores. These complexes exhibit interesting SMM properties that can be analysed based on some structural key features observed within a large family of related systems sharing the same metallic core.¹⁹ Inspired by the H₂mdea {Co(III)₂Dy(III)₂} complex,¹⁸ we have used the diethanolamine ligand and its *N*-alkyl derivatives (Scheme 1) to explore the effect of alkyl chain length on the structure and

magnetic behaviour of the resulting molecular assemblies. Surprisingly, under similar reaction conditions employed for the mdea {Co(III)₂Dy(III)₂} complex, the butterfly {Co(III)₂Dy(III)₂} core is not preserved in the crystallized products when N-C_ndea ligands are used in acetonitrile in combination with Co(II) pivalate and Dy(III) nitrate. For the C₄, C₆ and C₈ ligands, single crystals of hexanuclear {Co(III)₃Dy(III)₃} complexes are obtained (Fig. 1), while the crystalline products from the C₃ and C₁₀ ligands are not good enough for single-crystal X-ray structural determination. The infrared spectra of these complexes share a common fingerprint between 1300 and 1700 cm⁻¹ (Fig. 2), except for the C₃dea complex, 5-C₃. In fact, we collected enough evidence to determine that this complex possesses a butterfly structure {Co(III)₂Dy(III)₂} similar to the mdea analogue. Chemical analysis supports this formulation while the recrystallization of 5-C₃ in a methanol/acetonitrile mixture affords single crystals of [Co^{III}₂Dy^{III}₂(C₃-dea)₃(piv)₆(OCH₃)₂] (5-C_{3r}) (Fig. S1†), which possess a butterfly {Co(III)₂Dy(III)₂} core based on single-crystal X-ray diffraction data. This result shows that the crystalline solid obtained with C₃dea is different from the hexanuclear {Co(III)₃Dy(III)₃} complex isolated with longer alkyl chains. Further research will be necessary to confirm if this structural switching is driven only by the alkyl chain length of the C_n-dea ligand.

Single-crystal X-ray diffraction measurements show that complex 1-C₄ crystallizes in the monoclinic space group *Cc*, while complexes 2-C₆ and 3-C₈ crystallize in the monoclinic *P2₁/n* one. All complexes are heterometallic hexanuclear cages consisting of three Co^{III} and three Dy^{III} ions. The metal-oxo core in all complexes displays a hemicubane-like arrangement of the metal ions and oxygen atoms. The {Co₃Dy₃} moiety in this hexanuclear core is held by four μ₃-hydroxo groups. This structural motif can also be understood as a triangle-in-triangle arrangement with an inner {Dy₃} triangle and an outer {Co₃} one with a dihedral angle between triangle planes close to 40° (Fig. 3). The peripheral coordination sites are provided by the fully deprotonated C_n-H₂dea ligands (C_n-dea²⁻, denoted in the following as C_n-dea) that coordinate through the N atom

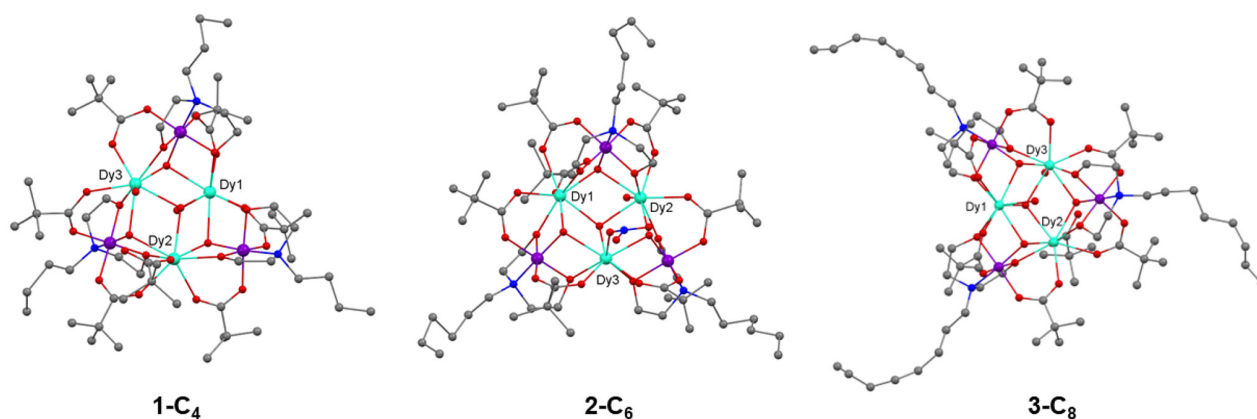


Fig. 1 Ball-and-stick representation of complexes 1-C₄, 2-C₆ and 3-C₈. Disordered atoms and H atoms were omitted for the sake of clarity. Green: Dy; violet: Co; red: O; blue: N; gray: C.

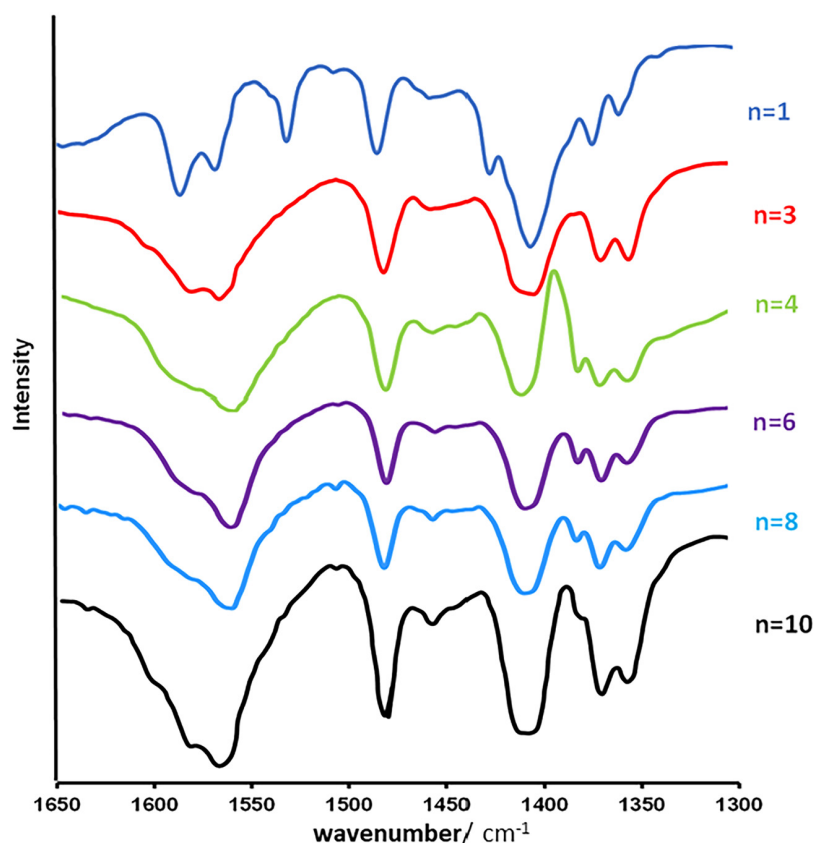


Fig. 2 KBr infrared spectra of reported complexes with different $N-C_n-H_2dea$ ligands, $\{Co(III)_2Dy(III)_2mdea\}$ ($n = 1$); $5-C_3$ ($n = 3$), $1-C_4$ ($n = 4$), $2-C_6$ ($n = 6$), $3-C_8$ ($n = 8$) and $4-C_{10}$ ($n = 10$).

to the Co^{III} ions and further bridge the Co^{III} centres to the Dy^{III} ions through its two μ -alkoxy groups and six μ -pivalate ligands. In fact, this hexanuclear $\{Co_3^{III}Dy_3^{III}(\mu_3-OH)_4(L)_3(piv)_6\}$ core has already been observed in two closely related cationic complexes, where $L =$ triethanolamine ($Co_3Dy_3tea_3$)²¹ and N -butyldiethanolamine ($Co_3Dy_3bdea_3$) with nitrate counterions.²⁰ The difference between these previously reported complexes and $1-C_4$, $2-C_6$ and $3-C_8$ resides in the three apical ligands (apical with respect to the Dy_3 triangle plane) fulfilling the Dy^{III} coordination spheres. While in $Co_3Dy_3tea_3$ and $Co_3Dy_3bdea_3$, these ligands are all water molecules, in $1-C_4$ and $3-C_8$, they are two aqua ligands and a κ^1O -pivalate ligand. On the other hand, in $2-C_6$, they are a water molecule, a κ^1O -pivalate ligand and a nitrate anion, making this complex neutral while $1-C_4$ and $3-C_8$ are mono-cationic complexes with nitrate as the counterion. In $2-C_6$, it looks like the nitrate counterion replaces the aqua ligand in the Dy coordination sphere. In fact, the nitrate counterion in $1-C_4$ and $3-C_8$ appears to be H-bonding to the aqua ligand making this interchange a feasible hypothesis (Fig. S2†). Another structural modification accompanied the nitrate/aqua interchange in $2-C_6$ with respect to $1-C_4$ and $3-C_8$, and the remaining aqua ligand exchanges its position with the κ^1O -pivalate ligand at the Dy site.

Regarding the alkyl chains of the C_n -dea ligands, even if they are highly disordered, they remain almost in the $\{Co_3\}$ triangle plane except for complex $2-C_6$ where they markedly tilt upwards (Fig. S3†).

In the three $\{Co(III)_3Dy(III)_3\}$ complexes, all three independent $Co(III)$ sites are six-coordinated in octahedral geometry with average $Co-O$ and $Co-N$ bond distances of 1.90(2) Å ($1-C_4$), 1.90(2) Å ($2-C_6$), 1.91(1) Å ($3-C_8$) and 1.97(2) Å ($1-C_4$), 1.94(3) Å ($2-C_6$), 2.00(2) Å ($3-C_8$), respectively. Regarding the three different $Dy(III)$ sites, they are eight-coordinated with different geometrical arrangements (Fig. S4†). According to SHAPE,²² complex $1-C_4$ shows bi-augmented trigonal prism (BTP) geometry (CShM, 0.690) at $Dy1$ and $Dy3$ sites while $Dy2$ exhibits a triangular dodecahedron (TDD) geometry (CShM, 0.842). Similarly, complex $3-C_8$ also shows BTP geometries (CShM, 0.719 and 0.692, respectively) at $Dy1$ and $Dy3$ sites and TDD geometry at the $Dy2$ site (CShM, 0.995). However, the geometry of $Dy2$ is also close to that of a BTP arrangement (CShM, 1.102 vs. 0.995 of TDD). On the other hand, complex $2-C_6$ shows the BTP arrangement at $Dy2$ and $Dy3$ sites (CShM, 0.808 and 0.972, respectively) in contrast to complexes $1-C_4$ and $3-C_8$ where this geometry corresponds to $Dy1$ and $Dy3$ sites. The $Dy1$ site here exhibits the SAP geometry (CShM, 0.544). These differences observed in complex $2-C_6$ are most probably related

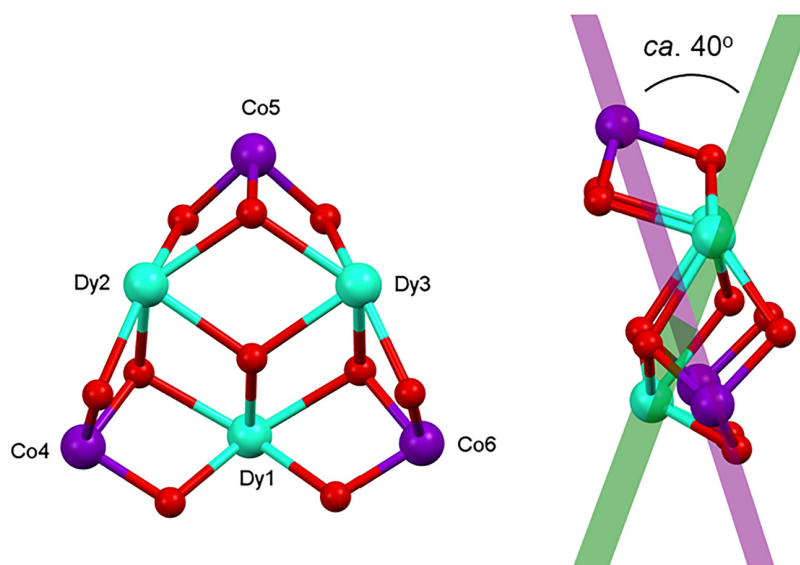


Fig. 3 $(\text{Co}^{\text{III}}\text{Dy}^{\text{III}})$ triangle-in-triangle core of the reported complexes and a view of the dihedral angle between the Co_3 and Dy_3 planes. Red balls correspond to oxygen atoms.

to the nitrate anion and aqua ligand interchange as previously mentioned (*vide supra*). The observed Dy–O bond lengths (Table S2†) show mean values ranging from 2.33(2) Å to 2.36(2) Å, which are almost identical at all sites in all complexes. The Dy–O bond lengths exhibit a remarkably narrow distribution across the three complexes, with variations between the maximum and minimum bond lengths ranging from 0.08 to 0.14 Å. An exception arises in complex 2-C₆, where the maximum–minimum bond length difference reaches 0.22 Å at the Dy2 site and 0.29 Å at the Dy3 site. Notably, this complex exhibits an unconventional short Dy–O bond distance of 2.15(3) Å at the Dy3 site, involving the alkoxide oxygen of the teaH^{2-} ligand. In general, across the three complexes, the Dy–O bond distances vary from 2.15(3) Å to 2.45(2) Å.

Regarding crystal packing, two main inter-molecular interactions can be distinguished in 1-C₄, 2-C₆ and 3-C₈. H-bond interactions involve the nitrate anion (as a counterion in 1-C₄ and 3-C₈; and as a coordinated ligand in 2-C₆), the coordinated aqua and hydroxo ligands of neighboring molecules as well as solvent water molecules (Fig. S5†). The other dominant interactions are C–H...C–H contacts between the *N*-alkyl chains and *tert*-butyl groups of pivalate ligands of the neighboring complexes (Fig. S6†). Both supramolecular interactions confer an ordering along a direction almost perpendicular to the packing (Fig. S7†). From the inter-play of these two dominant interactions, the shortest Dy...Dy inter-molecular distances are 10.530(2) Å in 1-C₄, 9.401(2) Å in 2-C₆ and 9.824(2) Å in 3-C₈ (Fig. S8†). In the case of the longer alkyl chains, the shortest Dy...Dy inter-molecular distance is driven by the C–H...C–H interactions, while the H-interaction in the 1-C₄ complex brings Dy sites to their closest distance. This aligns with the anticipated trend of strengthening C–H...C–H interactions as the alkyl chains lengthen. However, it is noteworthy that there

is no consistent, monotonous variation in the closest Dy...Dy inter-molecular distance with an increase in alkyl chain length.

Magnetic properties

Static dc susceptibility data. The temperature dependence of the dc magnetic susceptibility (χ) between 1.85 and 300 K at 1 kOe and the field dependence of the magnetization (M) up to 7 T in the 1.8–8 K range were recorded for the reported complexes. The χT product values at room temperature were estimated at 42.4, 42.0, 42.7 and 40.0 $\text{cm}^3 \text{K mol}^{-1}$ for 1-C₄, 2-C₆, 3-C₈ and 4-C₁₀, respectively, in good agreement with the expected value of 42.5 $\text{cm}^3 \text{K mol}^{-1}$ for three uncoupled Dy(III) centers (Dy(III): $S = 5/2$, $L = 5$, ${}^6\text{H}_{15/2}$, $\chi T = 14.17 \text{ cm}^3 \text{K mol}^{-1}$, $g = 4/3$ in a spherical symmetry; Co(III) is a closed-shell metal ion with $S = 0$). When lowering the temperature, the χT product decreases down to the lowest temperature, 1.8 K, to reach 18.4, 16.9, 12.9 and 25.0 $\text{cm}^3 \text{K mol}^{-1}$ for 1-C₄, 2-C₆, 3-C₈ and 4-C₁₀, respectively (Fig. 4). This behaviour is expected for the highly anisotropic Dy(III) center due to zero field splitting under symmetry lowering followed by Kramers doublets depopulation at the lower temperature range. The Kramers doublet (KD) energies and composition (in terms of $J = 15/2m_j$ states) are strongly dependent on the Dy(III) crystal field symmetry and strength. The overall χT vs. T profile below 50 K results from these KD composition and energy patterns. Reduced magnetization plots (M vs. H/T) down to 1.8 K and up to 7 T do not show clear saturation, nor do they exhibit isotherm superposition in agreement with the expected behaviour for the highly anisotropic Dy(III) ion. Maximum values registered at the lowest temperature (1.85 K) and the highest explored field (7 T) are 17.9, 17.0, 17.2 and 17.5 μ_{B} for complexes 1-C₄, 2-C₆, 3-C₈ and 4-C₁₀, respectively (Fig. 4).

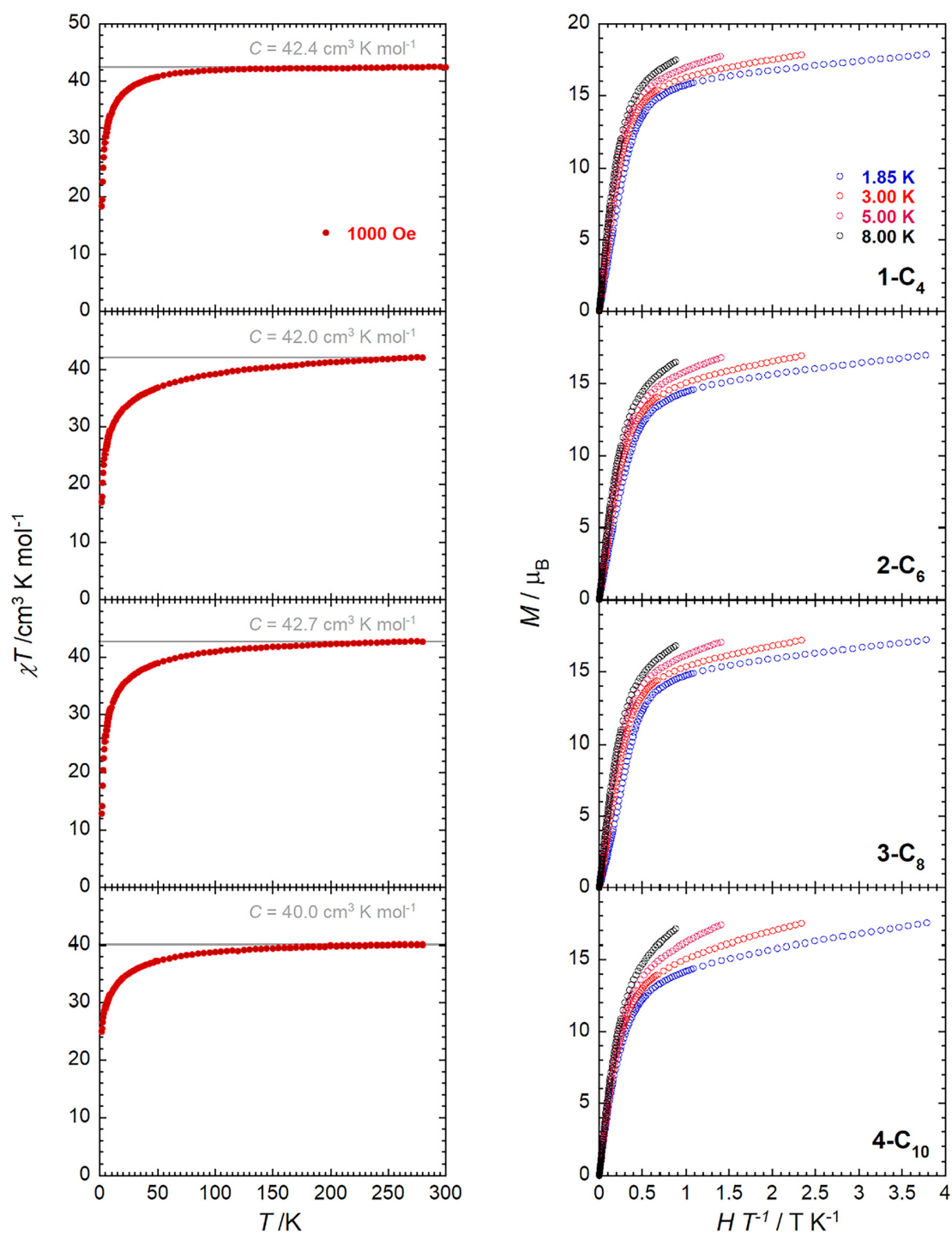


Fig. 4 Left: Temperature dependence of the χT product (χ is the molar dc susceptibility calculated from the ratio of the magnetization, M , and the applied magnetic field, H) at 0.1 T for 1-C₄, 2-C₆, 3-C₈ and 4-C₁₀. Right: Field dependence of the magnetization plotted as M vs. H/T for 1-C₄, 2-C₆, 3-C₈ and 4-C₁₀.

Dynamic ac susceptibility data. In order to test for possible slow relaxation of the magnetization in these complexes, ac susceptibility data were collected at low temperatures at driving frequencies up to 10 kHz in a zero-dc field. For all complexes, a detectable frequency- and temperature-dependent

out-of-phase signal (χ'') was observed below 10 K (Fig. 5 and S9†) evidencing the SMM properties of the reported complexes. However, a clear maximum of the relaxation mode in the χ'' vs. T and χ'' vs. ν plot in the zero-dc field was observed only in the case of 1-C₄, for which a second relaxation process

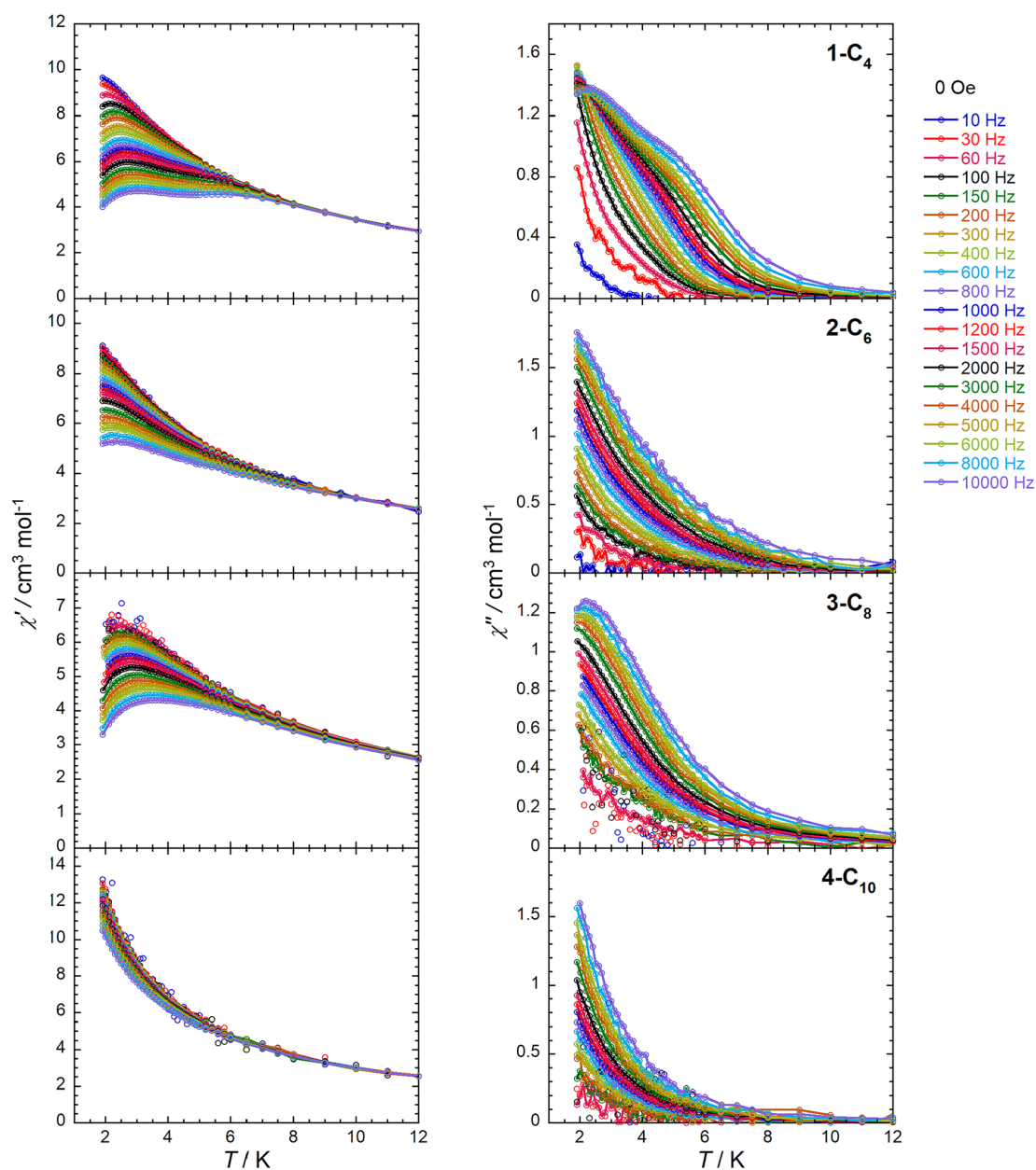


Fig. 5 Temperature dependence of the in-phase (left; χ') and out-of-phase (right; χ'') components of the ac susceptibility in the zero-dc field at indicated ac frequencies for **1-C₄**, **2-C₆**, **3-C₈** and **4-C₁₀**. Solid lines are guidance for the eyes.

could also be detected as a minor component (*vide infra*). For the other complexes, the magnetization relaxation is too fast even at 1.9 K, inducing a relaxation mode at frequencies higher than the instrumental limit value of 10 kHz. However, even if the characteristic frequency of the relaxation mode is not falling within the experimental window, the dynamic behaviour of the magnetization for these complexes can be discussed. As shown in Fig. 5 and S9,[†] **2-C₆** and **3-C₈** exhibit a characteristic frequency only slightly higher than 10 kHz at 1.9 K, while the relaxation mode in **4-C₁₀** is significantly at higher frequency as exemplified by the observation of only a

“tail” in the χ'' vs. T and χ'' vs. ν data profiles. At 1.9 K, the characteristic relaxation time of 7×10^{-4} , 1×10^{-5} , 2×10^{-5} and 1×10^{-6} s for **1-C₄**, **2-C₆**, **3-C₈** and **4-C₁₀**, respectively, were estimated when fitting the experimental χ'' vs. ν data to the generalized Debye model^{23,24} with a single relaxation mode (Table 1). This first analysis suggests that the elongation of the alkyl chain in the C_n -dea ligand promotes a faster magnetization relaxation.

In order to investigate further the magnetization dynamics of these complexes, the ac susceptibility was measured in the presence of a small dc field (up to 1 T) in order to suppress the

Table 1 Magnetization relaxation time best fitting parameters of the reported complexes

	1-C ₄			2-C ₆	3-C ₈	4-C ₁₀
$\sim\tau$ (1.9 K, 0 Oe)/s	7×10^{-4}			1×10^{-5}	2×10^{-5}	1×10^{-6}
Δ /K	τ_S only	τ_S	τ_F	—	58	—
τ_0 /s	38	37	77	—	—	—
n	7.8×10^{-8}	2.4×10^{-7}	3.8×10^{-11}	—	1.6×10^{-10}	—
$C/K^{-n} s^{-1}$	2.3	2.3	2.3	—	3.0	—
C_1/T^{-2}	350	340	1400	—	8100	—
C_2/T^{-2}	60	37	—	—	8.0	—
$A/T^{-4} K^{-1} s^{-1}$	510	520	—	—	810	—
	1.8×10^5	1.8×10^5	—	—	9.2×10^5	—

potential fast relaxation processes due to quantum tunneling of the magnetization. The expected field effect was not observable for 4-C₁₀ and only limited for 2-C₆ where the maximum of the relaxation mode stays very close to the ac frequency limit. On the other hand, the applied dc field shifts significantly the characteristic relaxation time at 2 K for 1-C₄, and 3-C₈ to lower frequencies offering the opportunity to study their magnetization dynamics in more detail (Fig. 6). For these two complexes, the temperature and frequency dependences of the ac susceptibility were recorded with an optimized dc field of 1000 Oe for 1-C₄ and 1500 Oe for 3-C₈, respectively (Fig. S10 and S11†).

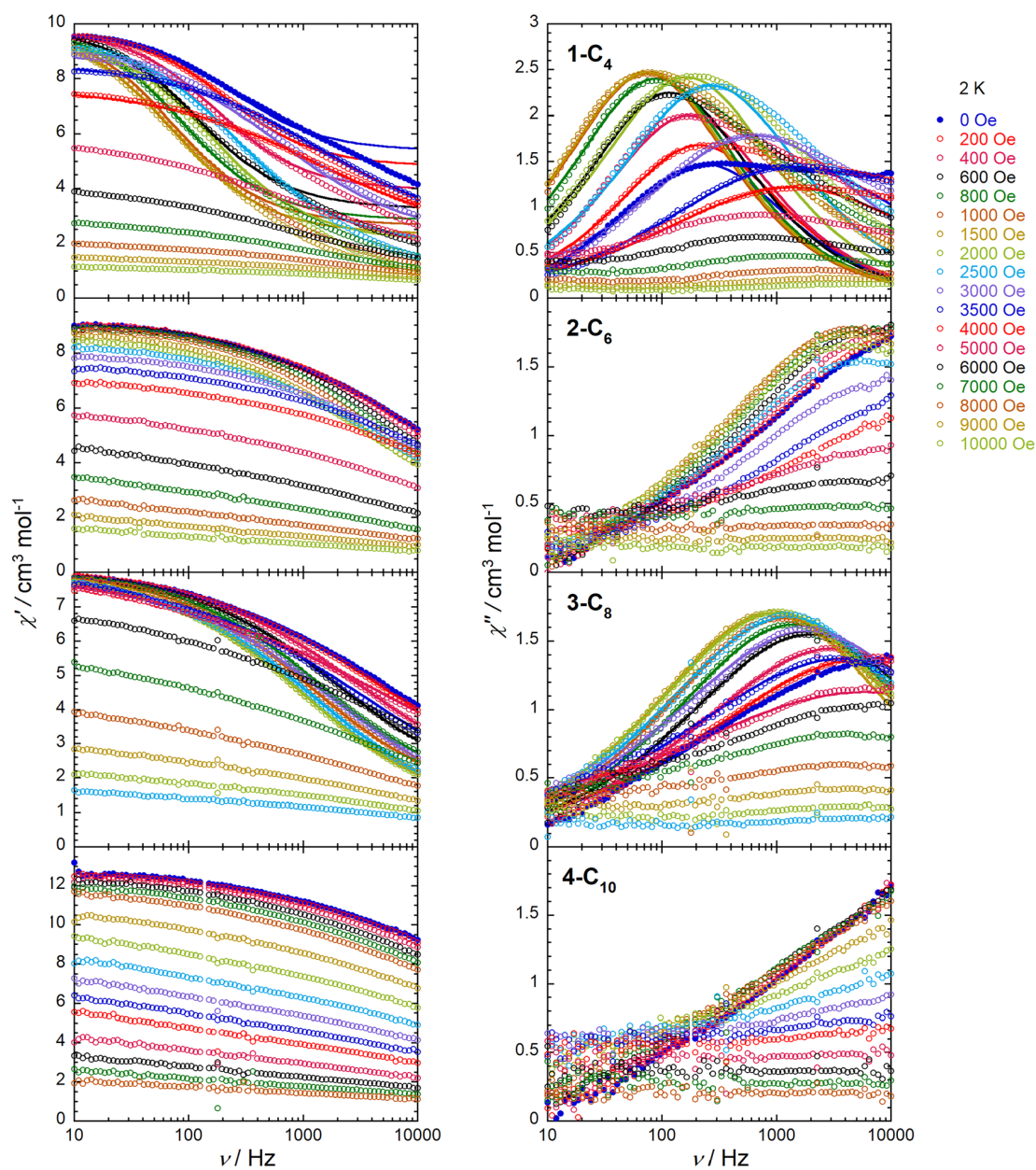


Fig. 6 Frequency dependence of the in-phase (left; χ') and out-of-phase (right; χ'') components of the ac susceptibility at 2 K and indicated dc field for 1-C₄, 2-C₆, 3-C₈ and 4-C₁₀. Solid lines are the best fits to the generalized Debye model.

As already mentioned above, the χ'' vs. ν plots in the zero-dc field for **1-C₄** (Fig. 6 and S9†) suggest the presence of at least two different relaxation modes with slow (τ_s) and fast (τ_f) relaxation times. This feature is less clear when applying a static dc field but still, a sum of two generalized Debye models is able to better reproduce the experimental data than those for a single generalized Debye model as exemplified by the corresponding Cole–Cole plots (Fig. S12†).²³ The presence of more than one relaxation process is most likely in relation to the presence of different Dy(III) sites in these complexes, in which Dy1 and Dy3 display very similar BTP coordination spheres (see Structural discussion), while the geometry of the remaining Dy2 differs clearly. Hence, these two different Dy(III) environments may explain the presence of two relaxation modes. Unfortunately, it was not possible to consider this model with two relaxation times for all the data sets of **1-C₄** when the fast relaxation time moves outside the experimental frequency window. The temperature and field evolution of the extracted relaxation times, considering one single mode (τ) and two modes (τ_s and τ_f) have been plotted and analysed (Fig. S13†). The first remark is that τ and τ_s are indeed very similar especially at low temperatures at which τ_f is not easy to estimate and to follow as a function of the dc field at 2 K. Thus, it implies that the field dependence of τ_f could not be fitted but is simply simulated (Fig. S13†) based on the relaxation model used to reproduce its temperature dependence

(Fig. 7). In the process to determine the different relaxation processes, it is clear that a fitting approach including two modes provides systematically a better agreement with the experimental data as expected with more adjustable parameters. Nevertheless, the single relaxation model appears to be the right choice for an easier comparison with **3-C₈**.

Both temperature and field dependences of the relaxation time for complexes **1-C₄** and **3-C₈** were modelled considering Raman, QTM (quantum tunnelling of the magnetization),²⁶ Direct, and Orbach-like relaxation processes (eqn (1)), which are often competing mechanisms in paramagnetic materials:²⁵

$$\tau^{-1} = \tau_{\text{Raman}}^{-1} + \tau_{\text{QTM}}^{-1} + \tau_{\text{Direct}}^{-1} + \tau_{\text{Orbach}}^{-1}$$

$$\tau^{-1} = C \frac{1 + C_1 H^2}{1 + C_2 H^2} T^n + \frac{B_1}{1 + B_2 H^2} + A T H^4 + \tau_0^{-1} \exp\left(-\frac{\Delta}{kT}\right) \quad (1)$$

For both complexes, the temperature and field evolution of their relaxation time is very similar (Fig. 7). The semi-logarithm τ vs. T^{-1} plots show a linear variation above 5 K, suggesting an Orbach-like mechanism. At lower temperature, there is no clear regime for which the relaxation time is a constant, implying that QTM relaxation can be neglected even in the zero-dc field for **1-C₄**. While the Direct mechanism is not operative in the zero-dc field, a Raman process should thus explain the variation of the relaxation below 5 K. Focusing on

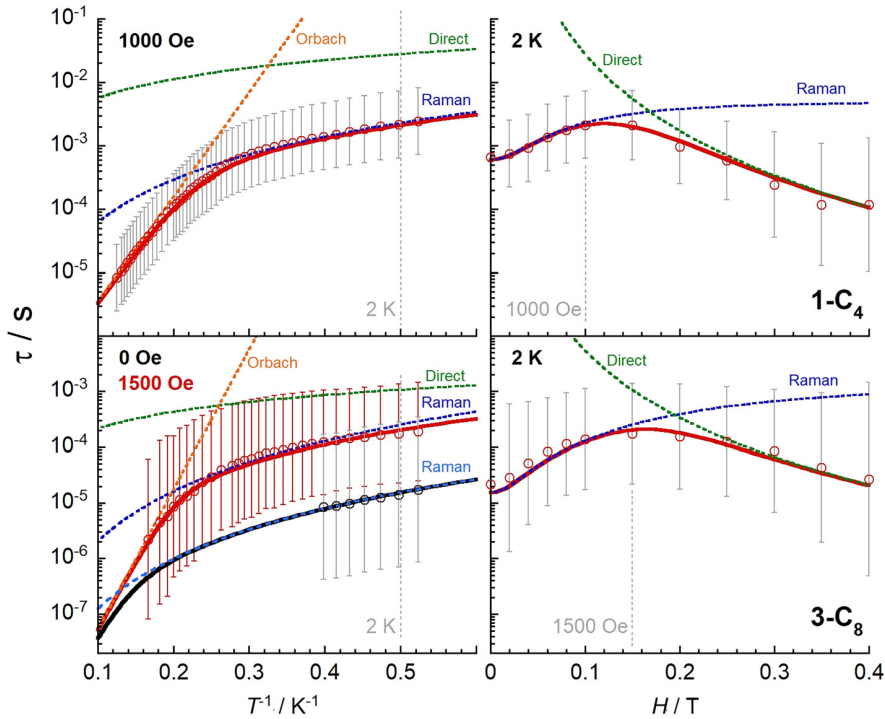


Fig. 7 Left: Temperature dependence of the relaxation time (plotted as τ vs. T^{-1} on a semi-logarithmic scale) at 1000 Oe for **1-C₄** (top), and at 0 and 1500 Oe for **3-C₈** (bottom). Right: Field dependence of the relaxation time (plotted as τ vs. H on a semi-logarithmic scale) at 2 K for **1-C₄** (top), and **3-C₈** (bottom). Solid lines are the best fits to the model considering a unique relaxation mode discussed in the text. Dotted lines are the Raman (blue), Direct (green) and Orbach (orange) components of the model.

the τ vs. H data, the increase of the relaxation at low fields, below around 0.15 T, agrees with a dominating Raman process, while at higher fields a Direct mechanism dominates and accelerates the magnetization relaxation. Therefore, Raman, Direct and Orbach-like mechanisms in eqn (1) were used to fit simultaneously field and temperature dependences of the relaxation time for both complexes **1-C₄** and **3-C₈**. As shown in Fig. 7 and S13,[†] this approach is able to reproduce extremely well the experimental data with the best fitting parameters listed in Table 1. The obtained thermal energy barriers of the Orbach-like process are 38 K, 37 K and 77 K for τ , τ_S and τ_E , respectively, for **1-C₄** while 58 K is found for **3-C₈**. These values are indeed quite small for paramagnetic Dy(III) ions, suggesting that low-energy vibrations may be involved in short-cutting the barrier energy.^{27,28} In fact, the low n exponent ($n = 2.3$ for **1-C₄** and $n = 3$ for **3-C₈**) of the Raman term reinforces this hypothesis and the potential role of low-energy vibrations in magnetization relaxation.²⁹ This complete analysis for **1-C₄** and **3-C₈** supports the hypothesis that the lengthening of the flexible pendant alkyl chains of the C_{*n*}-dea ligand could activate low-energy vibrations in the spin-phonon coupling and magnetization relaxation leading to an acceleration of the magnetization dynamics.

We have successfully prepared and structurally characterized a family of {Co₃Dy₃} complexes with a functionalized alcohol-amine ligand possessing a pendant N-C_{*n*}H_{2*n*+1} alkyl chain varying in length from $n = 4$ to $n = 10$. In contrast, the $n = 3$ ligand affords a different metallic core, with a butterfly {Co₂Dy₂} structure. Magnetic ac susceptibility data for this family of complexes demonstrate their SMM properties with relaxation times becoming faster with increasing *N*-alkyl chain length. The collected experimental data reveal the presence of competing Raman, Orbach-like and Direct relaxation mechanisms. The low value of the Orbach energy barrier as well as the low n exponent of the Raman process (see eqn (1)) strongly suggest the presence of low energy vibrations, which could accelerate the magnetization dynamics when increasing the alkyl chain length. The effect of the dipolar interactions between Dy sites does not seem to be relevant in this system as the inter-dysprosium distance does not change monotonously when increasing the alkyl chain length of the ligand. This contribution constitutes an initial study of the supramolecular control of magnetization dynamics by engineering peripheral ligands of SMM complexes, and more work is actually being developed in our laboratories toward this objective.

Materials and physical measurements

N-Alkyldiethanolamine ligands were prepared following a standard reported synthetic methodology.³⁰ Dysprosium nitrate

was prepared by reacting dysprosium oxide with nitric acid in aqueous solution. [Co₂(μ-OH₂)(μ-piv)₂(piv)₂(HPiv)₄], Hpiv = trimethylacetic acid, was prepared by following a previously reported procedure.³¹ All other chemicals were of reagent grade and used as received without further purification. Elemental analyses for C, H and N were performed with a Carlo Erba 1108 analyzer. FTIR spectra were recorded on a Nicolet iS10 FTIR spectrometer using KBr discs.

Preparation of the complex [Co^{III}Dy^{III}(C₄-dea)₃(piv)₇(OH)₄(H₂O)₂](NO₃), (**1-C₄**)

Co₂(OH₂)(Piv)₄(HPiv)₄ (0.09 g, 0.09 mmol) and Dy(NO₃)₃·xH₂O (0.054 g, 0.15 mmol) were dissolved in 10 mL of acetonitrile, followed by the addition of C₄-H₂dea (0.055 g, 0.40 mmol) and triethylamine (0.06 g, 0.60 mmol) dissolved in 10 mL of acetonitrile, affording a purple solution. The latter was then stirred for an hour, filtered off and allowed to stand sealed at room temperature. Within 3–4 weeks, a crop of violet crystals suitable for single-crystal X-ray measurements appeared. After picking up one specimen for X-ray data collection, the remaining crystals were filtered off, washed with acetonitrile and air dried.

Yield: 0.054 g (45%, Co based).

Anal. calcd. for C₅₉H₁₂₂Co₃Dy₃N₄O₂₉ (2015.92), C: 35.1, H: 6.1, N: 2.8. Found, C: 35.1, H: 6.5, N: 2.5.

Preparation of the complex [Co^{III}Dy^{III}(C₆-dea)₃(piv)₇(OH)₄(H₂O)(NO₃)], (**2-C₆**)

This complex was prepared following the same procedure as that for complex **1-C₄**, but employing the ligand C₆-H₂dea (0.081 g, 0.42 mmol).

Yield: 0.027 g (22%, Co based).

Anal. calcd for C₆₅H₁₃₂Co₃Dy₃N₄O₂₈ (2082.07), C: 37.5, H: 6.4, N: 2.7. Found, C: 37.3, H: 6.9, N: 2.5.

Preparation of the complex [Co^{III}Dy^{III}(C₈-dea)₃(piv)₇(OH)₄(H₂O)₂](NO₃), (**3-C₈**)

This complex was prepared following the same procedure as that for complex **1-C₄**, but employing the ligand C₈-H₂dea (0.086 g, 0.40 mmol).

Yield: 0.030 g (23%, Co based).

Anal. calcd for C₇₁H₁₄₆Co₃Dy₃N₄O₂₉ (2184.25), C: 39.0, H: 6.7, N: 2.6. Found, C: 38.9, H: 6.5, N: 2.5.

Preparation of the complex [Co^{III}Dy^{III}(C₁₀-dea)₃(piv)₇(OH)₄(H₂O)(NO₃)], (**4-C₁₀**)

This complex was prepared following the same procedure as that for complex **1-C₄**, but employing the ligand C₁₀-H₂dea (0.098 g, 0.42 mmol). In this case, the crystalline product was not suitable for single-crystal X-ray characterization.

Yield: 0.042 g (31%, Co based).

Anal. calcd for C₇₇H₁₅₆Co₃Dy₃N₄O₂₈ (2250.39), C: 41.1, H: 7.0, N: 2.5. Found, C: 41.8, H: 7.3, N: 2.0.

Preparation of the complex $[\text{Co}^{\text{III}}\text{Dy}^{\text{III}}(\text{C}_3\text{-dea})_3(\text{piv})_6(\text{OH})_2]\cdot 2\text{H}_2\text{O}$, (5-C₃)

This complex was prepared following the same procedure as that for complex 1-C₄, but employing the ligand C₃-H₂dea (0.058 g, 0.4 mmol). In this case, the crystalline product was not suitable for single-crystal X-ray characterization.

Yield: 0.075 g (59%, Co based).

Anal. calcd for C₄₄H₈₈Co₂Dy₂N₂O₁₈ (1410.06), C: 37.5, H: 6.4, N: 2.0. Found, C: 37.1, H: 6.6, N: 1.9.

For comparison, the calculated chemical analysis of the hypothetical {Co₃Dy₃} complex, $[\text{Co}_3^{\text{III}}\text{Dy}_3^{\text{III}}(\text{C}_3\text{-dea})_3(\text{piv})_7(\text{OH})_4(\text{H}_2\text{O})_2](\text{NO}_3)$ should have been: C₅₆H₁₁₄Co₃Dy₃N₄O₂₈ (1973.84), C: 34.1, H: 5.9, N: 2.8.

After recrystallization from a methanol/acetonitrile mixture, blue crystals suitable for single-crystal X-ray characterization appeared, resulting in the complex $[\text{Co}_2^{\text{III}}\text{Dy}_2^{\text{III}}(\text{C}_3\text{-dea})_3(\text{piv})_6(\text{OCH}_3)_2]$, 5-C_{3r}. No further characterization of these species was performed.

Magnetic measurements

The magnetic measurements were carried out in the temperature range between 1.85 and 300 K with applied dc fields ranging from -7 to +7 T, using an MPMS-XL Quantum Design SQUID magnetometer and a PPMS-9 Quantum Design susceptometer. The measurements were performed on polycrystalline samples, covered with immersion oil and enclosed in a sealed polyethylene bag. Prior to the experiments, the field-dependent magnetization was measured at 100 K to confirm the absence of any bulk ferromagnetic impurities. The ac susceptibility data have been collected between 10 and 10 000 Hz with ac fields ranging from 1 to 6 Oe and dc fields ranging between 0 and 1 T. The magnetic data were corrected for the diamagnetic contributions from the sample and sample holder.

X-ray structure determination

The crystal structures of 1-C₄, 2-C₆, 3-C₈ and 5-C_{3r} were determined with an Oxford Xcalibur, Eos, Gemini CCD area-detector diffractometer using graphite-monochromated Mo-K α radiation ($\lambda = 0.71069 \text{ \AA}$) at 298 K. Crystals were directly obtained from the synthetic procedure (except for recrystallized 5-C_{3r}) and were picked up prior to filtering and drying. Data were corrected for absorption with CrysAlisPro, Oxford Diffraction Ltd, Version 1.171.33.66, applying an empirical absorption correction using spherical harmonics, implemented in the SCALE3 ABSPACK scaling algorithm.³² The structures were solved by direct methods with SHELXT³³ and refined by full-matrix least-squares on F^2 with SHELXL-2014³⁴ under the WinGX³⁵ platform. Hydrogen atoms were added geometrically and refined as riding atoms with a uniform value of U_{iso} . In all structures, most of the pivalate methyl groups as well as C_n-dea ligand methylene groups and the nitrate anion were found disordered around two positions and were refined with 0.5 : 0.5 fixed occupancy factors. The alkyl chain carbon atoms of C_n-dea ligands were also found to be strongly disordered and were refined as split positions with 0.5 : 0.5 fixed occupancy factors adding

similarity restraints to the C-C bond distances to keep the refinement stable. H atoms of water molecules and hydroxide ligands were geometrically added by relying on H-bond patterns and refined with O-H distance constraints and fixed $U_{\text{iso}} = 1.5U_{\text{iso}}$ of the bound O atom.

We gratefully acknowledge the UBA, ANPCYT and CONICET for funding resources. PA and FDC are staff members of the CONICET. NV is a post-doctoral fellow of CONICET. ChB thanks the Région Grand Est (France) for an Erasmus fellowship. R. C. and M. R. thank the University of Bordeaux the Région Nouvelle Aquitaine, Quantum Matter Bordeaux (QMBx), the Centre National de la Recherche Scientifique (CNRS), and the Association Francaise de Magnétisme Moléculaire.

- 1 D. Gatteschi, R. Sessoli and J. Villain, *Molecular Nanomagnets*, Oxford University Press, 2006.
- 2 M. Affronte, *J. Mater. Chem.*, 2009, **19**, 1731–1737.
- 3 D. N. Woodruff, R. E. P. Winpenny and R. A. Layfield, *Chem. Rev.*, 2013, **113**, 5110–5148.
- 4 P. Zhang, L. Zhang and J. Tang, *Dalton Trans.*, 2015, **44**, 3923–3929.
- 5 A. Dey, P. Kalita and V. Chandrasekhar, *ACS Omega*, 2018, **3**, 9462–9475.
- 6 L. Rosado Piquer and E. C. Sañudo, *Dalton Trans.*, 2015, **44**, 8771–8780.
- 7 P. Zhang, Y.-N. Guo and J. Tang, *Coord. Chem. Rev.*, 2013, **257**, 1728–1763.
- 8 Y.-C. Chen, J.-L. Liu, L. Ungur, J. Liu, Q.-W. Li, L.-F. Wang, Z.-P. Ni, L. F. Chibotaru, X.-M. Chen and M.-L. Tong, *J. Am. Chem. Soc.*, 2016, **138**, 2829–2837.
- 9 C. A. P. Goodwin, F. Ortu, D. Reta, N. F. Chilton and D. P. Mills, *Nature*, 2017, **548**, 439–442.
- 10 F.-S. Guo, B. M. Day, Y.-C. Chen, M.-L. Tong, A. Mansikkamäki and R. A. Layfield, *Science*, 2018, **362**, 1400–1403.
- 11 S. K. Langley, N. F. Chilton, L. Ungur, B. Moubaraki, L. F. Chibotaru and K. S. Murray, *Inorg. Chem.*, 2012, **51**, 11873–11881.
- 12 S. K. Langley, N. F. Chilton, B. Moubaraki and K. S. Murray, *Chem. Commun.*, 2013, **49**, 6965.

- 13 A. V. Funes, L. Carrella, E. Rentschler and P. Alborés, *Dalton Trans.*, 2014, **43**, 2361–2364.
- 14 S. K. Langley, L. Ungur, N. F. Chilton, B. Moubaraki, L. F. Chibotaru and K. S. Murray, *Inorg. Chem.*, 2014, **53**, 4303–4315.
- 15 S. K. Langley, N. F. Chilton, B. Moubaraki and K. S. Murray, *Inorg. Chem. Front.*, 2015, **2**, 867–875.
- 16 A. V. Funes, L. Carrella, Y. Rechkemmer, J. van Slageren, E. Rentschler and P. Alborés, *Dalton Trans.*, 2017, **46**, 3400–3409.
- 17 K. R. Vignesh, S. K. Langley, K. S. Murray and G. Rajaraman, *Inorg. Chem.*, 2017, **56**, 2518–2532.
- 18 A. V. Funes, M. Perfetti, M. Kern, N. Rußegger, L. Carrella, E. Rentschler, J. Slageren and P. Alborés, *Eur. J. Inorg. Chem.*, 2021, **2021**, 3191–3210.
- 19 A. V. Funes and P. Alborés, *Eur. J. Inorg. Chem.*, 2018, **2018**, 2067–2089.
- 20 J. A. Sheikh, S. Goswami and S. Konar, *Dalton Trans.*, 2014, **43**, 14577–14585.
- 21 I. Radu, V. Ch. Kravtsov, S. M. Ostrovsky, O. S. Reu, K. Krämer, S. Decurtins, S.-X. Liu, S. I. Klokishner and S. G. Baca, *Inorg. Chem.*, 2017, **56**, 2662–2676.
- 22 S. Alvarez, P. Alemany, D. Casanova, J. Cirera, M. Llunell and D. Avnir, *Coord. Chem. Rev.*, 2005, **249**, 1693–1708.
- 23 K. S. Cole and R. H. Cole, *J. Chem. Phys.*, 1941, **9**, 341–351.
- 24 H. B. G. Casimir and F. K. du Pré, *Physica*, 1938, **5**, 507–511.
- 25 K. N. Shrivastava, *Phys. Status Solidi B*, 1983, **117**, 437–458.
- 26 S. K. Misra, in *Multifrequency Electron Paramagnetic Resonance*, ed. S. K. Misra, Wiley, 1st edn, 2011, pp. 845–874.
- 27 A. Lunghi, F. Totti, S. Sanvito and R. Sessoli, *Chem. Sci.*, 2017, **8**, 6051–6059.
- 28 L. Escalera-Moreno, N. Suaud, A. Gaita-Ariño and E. Coronado, *J. Phys. Chem. Lett.*, 2017, **8**, 1695–1700.
- 29 L. Gu and R. Wu, *Phys. Rev. B*, 2021, **103**, 014401.
- 30 M. Mascal, I. Yakovlev, E. B. Nikitin and J. C. Fettinger, *Angew. Chem., Int. Ed.*, 2007, **46**, 8782–8784.
- 31 G. Aromí, A. S. Batsanov, P. Christian, M. Helliwell, A. Parkin, S. Parsons, A. A. Smith, G. A. Timco and R. E. P. Winpenny, *Chem. – Eur. J.*, 2003, **9**, 5142–5161.
- 32 *SCALE3 ABSPACK: Empirical absorption correction, CrysAlis – Software package*, 2006.
- 33 G. M. Sheldrick, *Acta Crystallogr., Sect. A: Found. Adv.*, 2015, **71**, 3–8.
- 34 G. M. Sheldrick, *Acta Crystallogr., Sect. A: Found. Crystallogr.*, 2008, **64**, 112–122.
- 35 L. J. Farrugia, *J. Appl. Crystallogr.*, 2012, **45**, 849–854.

Supplementary Information

Alkyl chain length influence of the functionalized diethanolamine ligand on the slow relaxation of the magnetization in $\{\text{Co}^{\text{III}}_3\text{Dy}^{\text{III}}_3\}$

**Chl e Bonenfant^[a,b], Nahir Vadra^[a], Mathieu Rouzier s^[c], Rodolphe Cl rac^[c],
Fabio D. Cukiernik^{[a]*} and Pablo Albor s^{[a]*}**

[a] Departamento de Qu mica Inorg nica, An lica y Qu mica F sica/ INQUIMAE (CONICET), Facultad de Ciencias Exactas y Naturales Universidad de Buenos Aires, Pabell n 2, Ciudad Universitaria, C1428EHA Buenos Aires, Argentina
Fax: +5411 / 4576-3341

e-mail: albores@qi.fcen.uba.ar; fabioc@qi.fcen.uba.ar

[b] On leave from Ecole Europ ene d'Ing nieurs de Chimie, Polym res et Mat riaux, Universit  de Strasbourg, France.

[c] Univ. Bordeaux, CNRS, CRPP, UMR 5031, 33600 Pessac, France.

Table S1. Main crystallographic data of the reported complexes.

	1-C₄	2-C₆	3-C₈	5-C_{3r}
Empirical Formula	C ₅₉ H ₁₂₂ Co ₃ Dy ₃ N ₄ O ₂₉	C ₆₅ H ₁₃₄ Co ₃ Dy ₃ N ₄ O ₂₉	C ₇₁ H ₁₄₈ Co ₃ Dy ₃ N ₄ O ₃₀	C ₄₆ H ₉₀ Co ₂ Dy ₂ N ₂ O ₁₈
Formula weight	2014.88	2100.04	2202.22	1402.05
<i>T</i> (K)	293 (2)	293 (2)	293 (2)	293 (2)
Crystal system	Monoclinic	Monoclinic	Monoclinic	Monoclinic
Space Group	<i>Cc</i>	<i>P2₁/c</i>	<i>P2₁/c</i>	<i>P2₁/c</i>
<i>a</i> (Å)	16.3759(4)	25.5185(18)	28.532(2)	16.1479(5)
<i>b</i> (Å)	19.4907(5)	19.1773(11)	10.5787(10)	14.3681(6)
<i>c</i> (Å)	27.2707(6)	18.9054(11)	33.001(3)	25.5601(8)
α (°)	90	90	90	90
β (°)	90.159(2)	93.943(6)	93.753(7)	93.754(3)
γ (°)	90	90	90	90
<i>V</i> (Å ³)	8704.2(4)	9229.9(10)	9939(1)	5917.6(4)
<i>Z</i>	4	4	4	4
<i>D</i> _{calc} (mg/m ³)	1.538	1.511	1.472	1.574
Absorption coefficient (mm ⁻¹)	3.171	2.994	2.785	3.111
<i>F</i> (000)	4056	4252	4484	2840
λ (Å)	0.71073	0.71073	0.71073	0.71073
θ Range data collection (°)	3.3 – 27.0	3.7 – 23.0	3.6 – 27.0	3.7 – 27.0
Index ranges	-20 ≤ <i>h</i> ≤ 17	-32 ≤ <i>h</i> ≤ 30	-36 ≤ <i>h</i> ≤ 36	-20 ≤ <i>h</i> ≤ 20
	-24 ≤ <i>k</i> ≤ 24	-17 ≤ <i>k</i> ≤ 24	-13 ≤ <i>k</i> ≤ 13	-18 ≤ <i>k</i> ≤ 17
	-34 ≤ <i>l</i> ≤ 34	-24 ≤ <i>l</i> ≤ 23	-27 ≤ <i>l</i> ≤ 42	-32 ≤ <i>l</i> ≤ 31
Reflections collected/unique	25479 / 13127	41144 / 19693	51992 / 21276	28678 / 12689
<i>R</i> _{int}	0.0429	0.1111	0.1210	0.0484
Observed reflections [<i>I</i> > 2σ(<i>I</i>)]	10271	9691	11740	8498
Completeness (%)	99.7	99.6	99.4	99.7
Maximum / minimum transmission	0.689 / 1.000	0.534 / 1.000	0.461 / 1.000	0.630 / 1.000
Data/restraints/parameters	13127 / 668 / 928	19693 / 1834 / 1037	21276 / 819 / 1097	12689 / 348 / 615
Goodness-of-fit (GOF) on <i>F</i> ²	1.017	1.059	1.057	1.039
Final <i>R</i> -index [<i>I</i> > 2σ(<i>I</i>)] / all data	0.069 / 0.098	0.1788 / 0.2785	0.1157 / 0.1882	0.0551 / 0.0926
<i>wR</i> index [<i>I</i> > 2σ(<i>I</i>)] / all data	0.194 / 0.242	0.3750 / 0.4413	0.2672 / 0.3355	0.1282 / 0.1559
Largest peak and hole (e Å ⁻³)	2.415 and -0.987	5.356 and -4.911	3.488 and -2.504	1.912 and -1.601
Weights, <i>w</i>	1/[σ ² (<i>F</i> _o ²) + (0.1410 <i>P</i>) ² + 136.5640 <i>P</i>] where <i>P</i> =(<i>F</i> _o ² +2 <i>F</i> _c ²)/3	1/[σ ² (<i>F</i> _o ²) + 1274.4493 <i>P</i>] where <i>P</i> =(<i>F</i> _o ² +2 <i>F</i> _c ²)/3	1/[σ ² (<i>F</i> _o ²) + (0.1109 <i>P</i>) ² + 192.2491 <i>P</i>] where <i>P</i> =(<i>F</i> _o ² +2 <i>F</i> _c ²)/3	1/[σ ² (<i>F</i> _o ²) + (0.0513 <i>P</i>) ² + 43.2064 <i>P</i>] where <i>P</i> =(<i>F</i> _o ² +2 <i>F</i> _c ²)/3

Table S2. Dy-O bond distances (Å) of reported complexes.

1-C ₄			2-C ₆			3-C ₈			
	O22	Dy1	2.31(2)	O9	Dy1	2.25(2)	O8	Dy1	2.27(1)
	O6	Dy1	2.32(2)	O10	Dy1	2.28(2)	O9	Dy1	2.29(1)
	O8	Dy1	2.34(2)	O11A	Dy1	2.32(2)	O15	Dy1	2.32(1)
	O3	Dy1	2.36(2)	O16	Dy1	2.33(3)	O14	Dy1	2.38(1)
	O23	Dy1	2.37(2)	O17	Dy1	2.33(3)	O26	Dy1	2.38(1)
	O9	Dy1	2.37(2)	O1	Dy1	2.35(2)	O4	Dy1	2.385(9)
	O1	Dy1	2.39(2)	O3	Dy1	2.36(2)	O2	Dy1	2.388(9)
	O15	Dy1	2.45(2)	O2	Dy1	2.39(2)	O3	Dy1	2.40(1)
mean			2.36(2)			2.33(2)			2.35(1)
max-min			0.14(2)			0.14(2)			0.13(1)
	O20	Dy2	2.29(2)	O8	Dy2	2.22(2)	O6	Dy2	2.32(1)
	O11	Dy2	2.31(2)	O4	Dy2	2.26(2)	O20	Dy2	2.32(1)
	O10	Dy2	2.34(2)	O7	Dy2	2.34(2)	O21	Dy2	2.34(1)
	O25	Dy2	2.36(2)	O24	Dy2	2.37(3)	O7	Dy2	2.35(1)
	O24	Dy2	2.36(2)	O1	Dy2	2.37(2)	O18	Dy2	2.37(1)
	O1	Dy2	2.38(2)	O27	Dy2	2.39(2)	O4	Dy2	2.372(9)
	O5	Dy2	2.38(2)	O25	Dy2	2.41(3)	O2	Dy2	2.381(9)
	O3	Dy2	2.39(2)	O2	Dy2	2.44(2)	O1	Dy2	2.40(1)
mean			2.35(2)			2.35(2)			2.36(1)
max-min			0.10(2)			0.22(2)			0.08(1)
	O13	Dy3	2.29(2)	O6	Dy3	2.15(3)	O5	Dy3	2.28(1)
	O2	Dy3	2.31(2)	O5	Dy3	2.28(2)	O10	Dy3	2.29(1)
	O18	Dy3	2.32(2)	O20	Dy3	2.29(3)	O2	Dy3	2.35(1)
	O12	Dy3	2.35(2)	O21	Dy3	2.34(2)	O24	Dy3	2.35(1)
	O1	Dy3	2.38(2)	O1	Dy3	2.38(2)	O11	Dy3	2.36(1)
	O9	Dy3	2.39(1)	O14	Dy3	2.39(2)	O1	Dy3	2.36(1)
	O5	Dy3	2.40(2)	O3	Dy3	2.44(2)	O3	Dy3	2.384(9)
	O27	Dy3	2.41(2)	O4	Dy3	2.44(2)	O25	Dy3	2.42(1)
mean			2.36(2)			2.34(2)			2.35(1)
max-min			0.12(2)			0.29(2)			0.14(1)

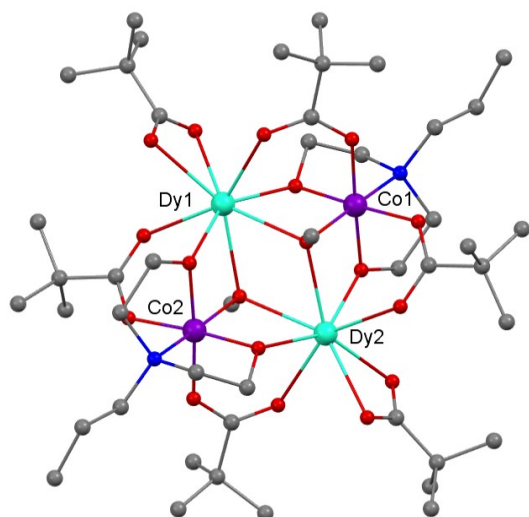


Figure S1. Ball and stick molecular representation of complex **5-C_{3r}**. Disordered atoms and H atoms were omitted for sake of clarity.

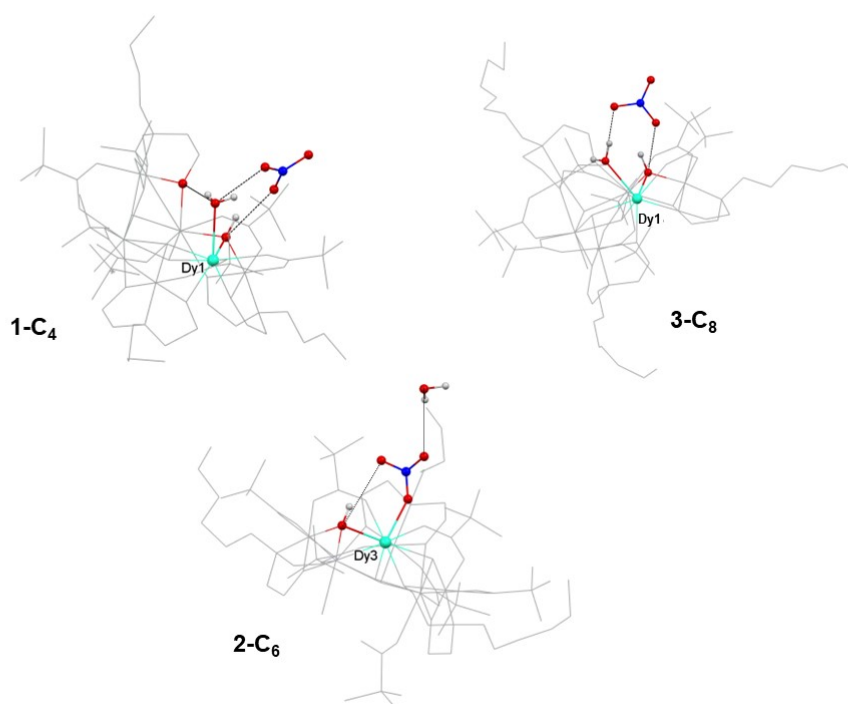


Figure S2. Intra-molecular H-bond interaction involving the nitrate ion as ligand and counterion in the reported complexes. Red: O; Blue: N; White: H. Molecule backbone in gray wireframes.

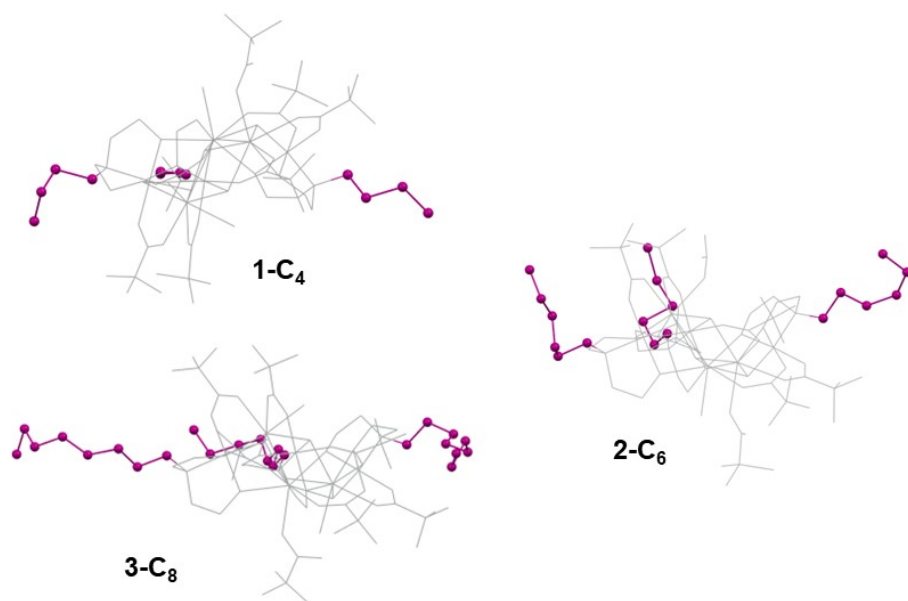


Figure S3. Alkyl chains orientation with respect to molecular plane in the reported complexes.

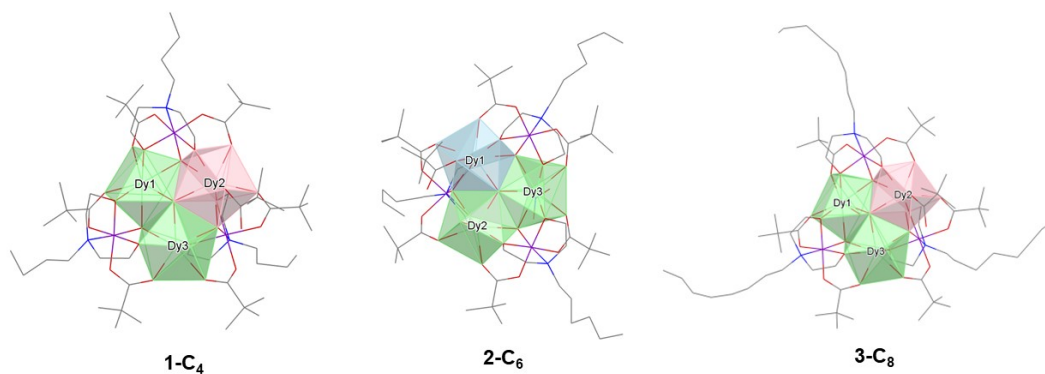


Figure S4. Polyhedral representation of Dy(III) sites in the reported complexes. Colours reflect closest geometrical symmetry according to CShM values (see text). Light green: BTP; pink: TDD and light blue: SAP.

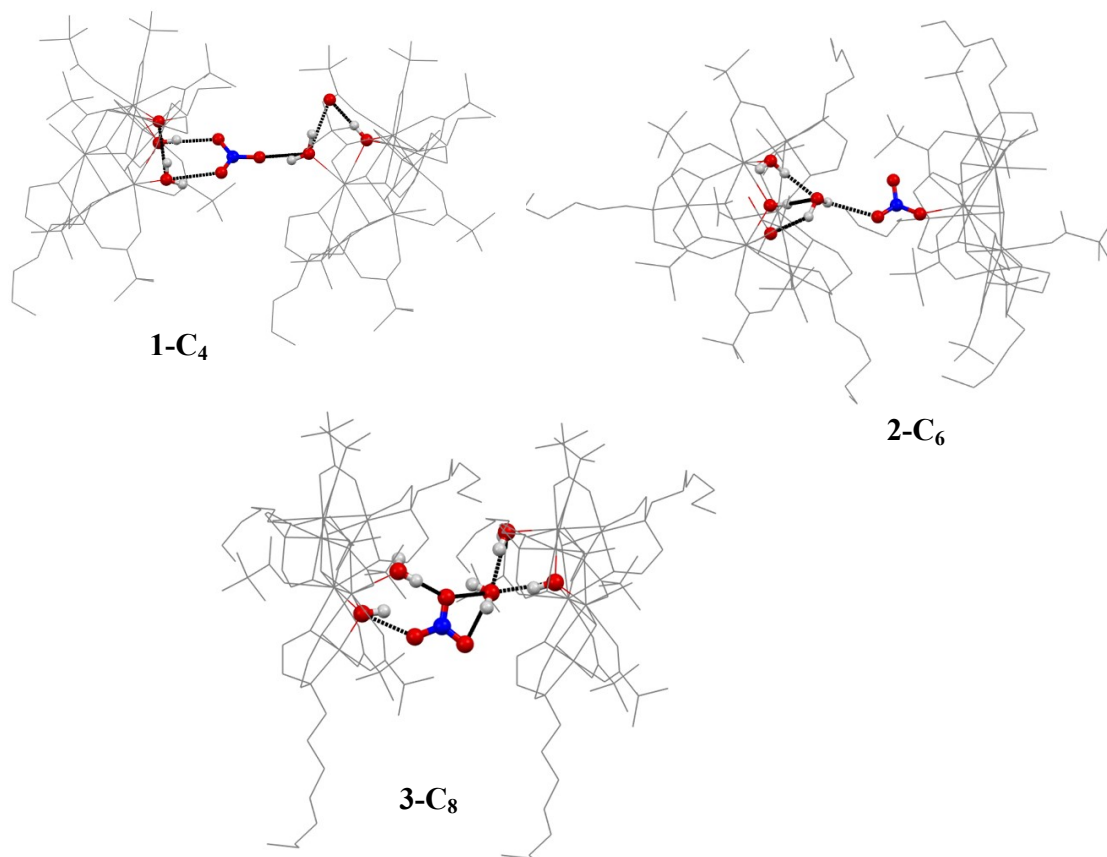


Figure S5. Inter-molecular H-interaction mediated by the nitrate counterion (ligand in 2-C₆). H atoms omitted for sake of clarity except for the ones involved in the H-bonding. Red: oxygen; Blue: nitrogen; White: hydrogen.

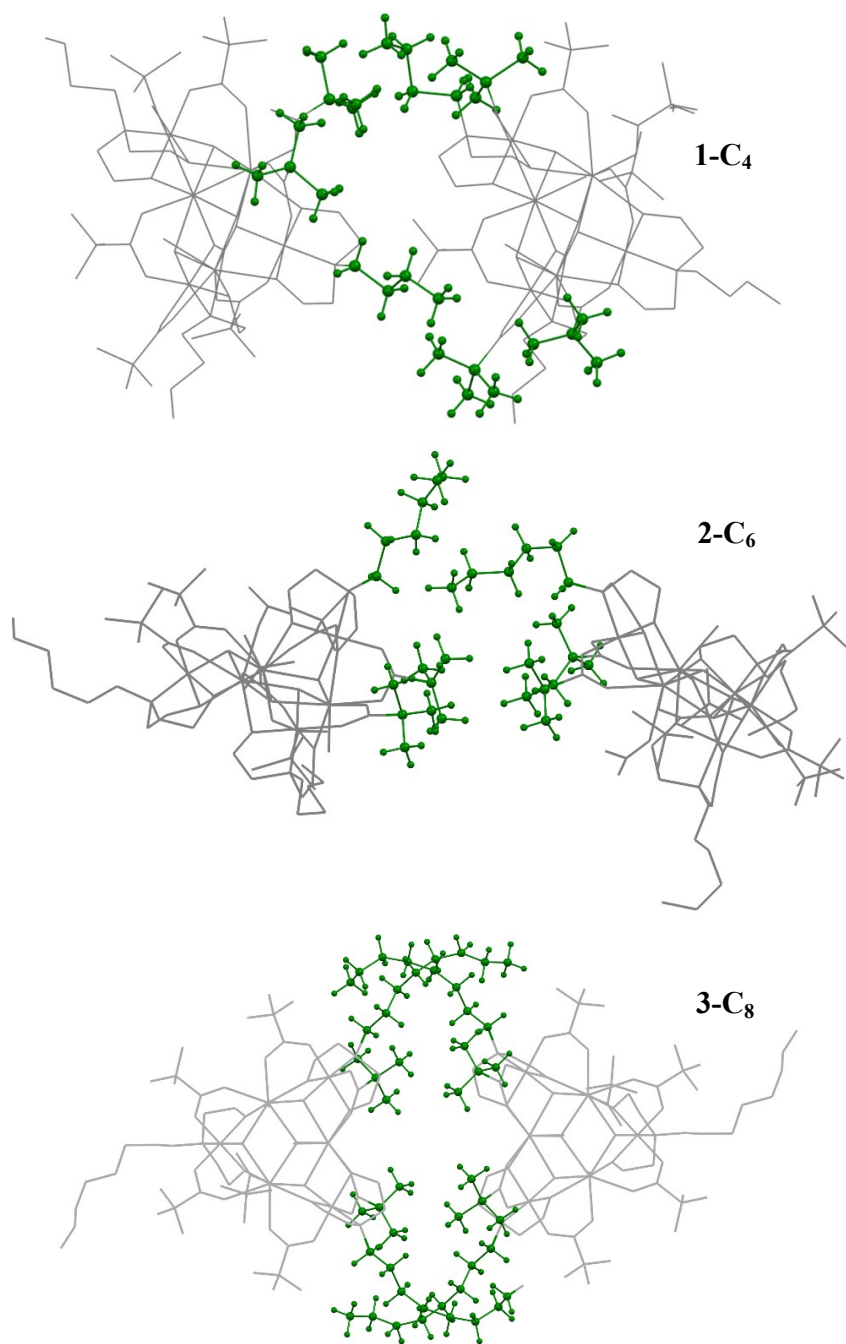
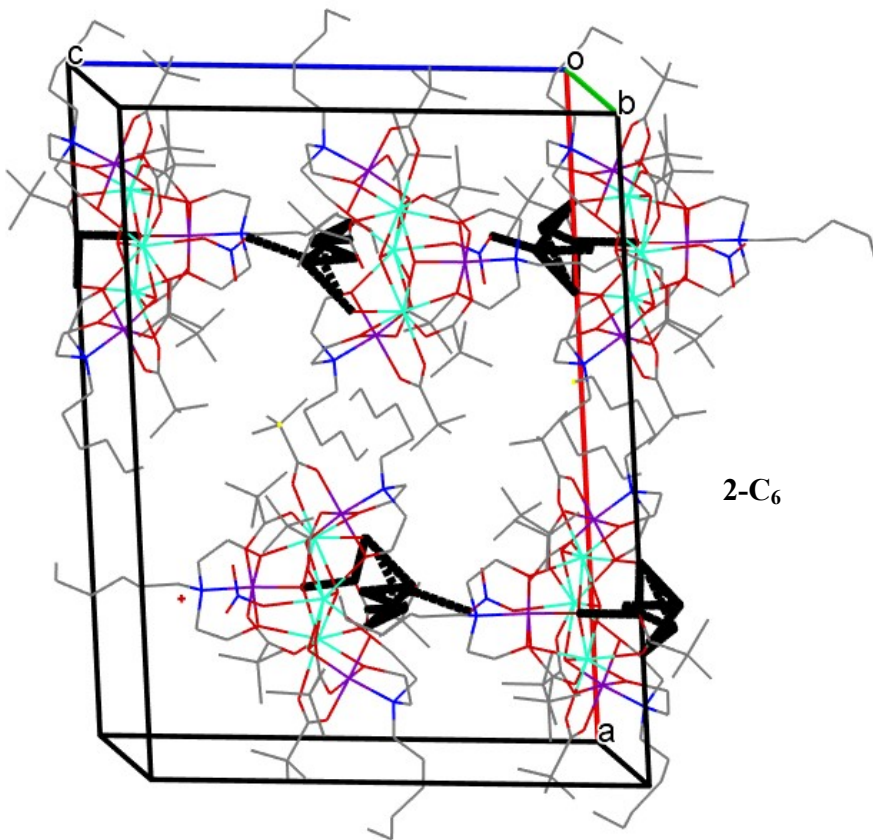
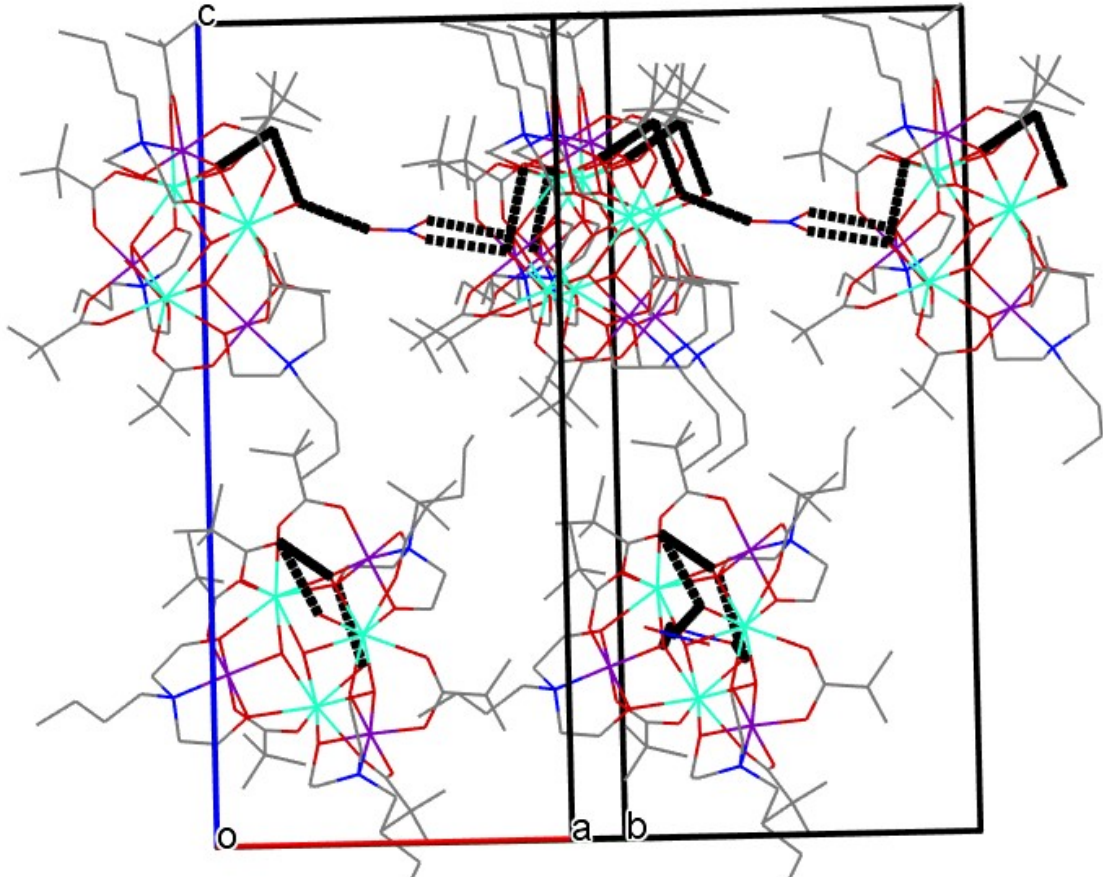


Figure S6. Inter-molecular C-H...C-H interactions mediated by the alkyl chains and pivalate *tert*-butyl groups (green). H atoms omitted for sake of clarity except for the ones involved in the inter-molecular interaction.

1-C₄



2-C₆

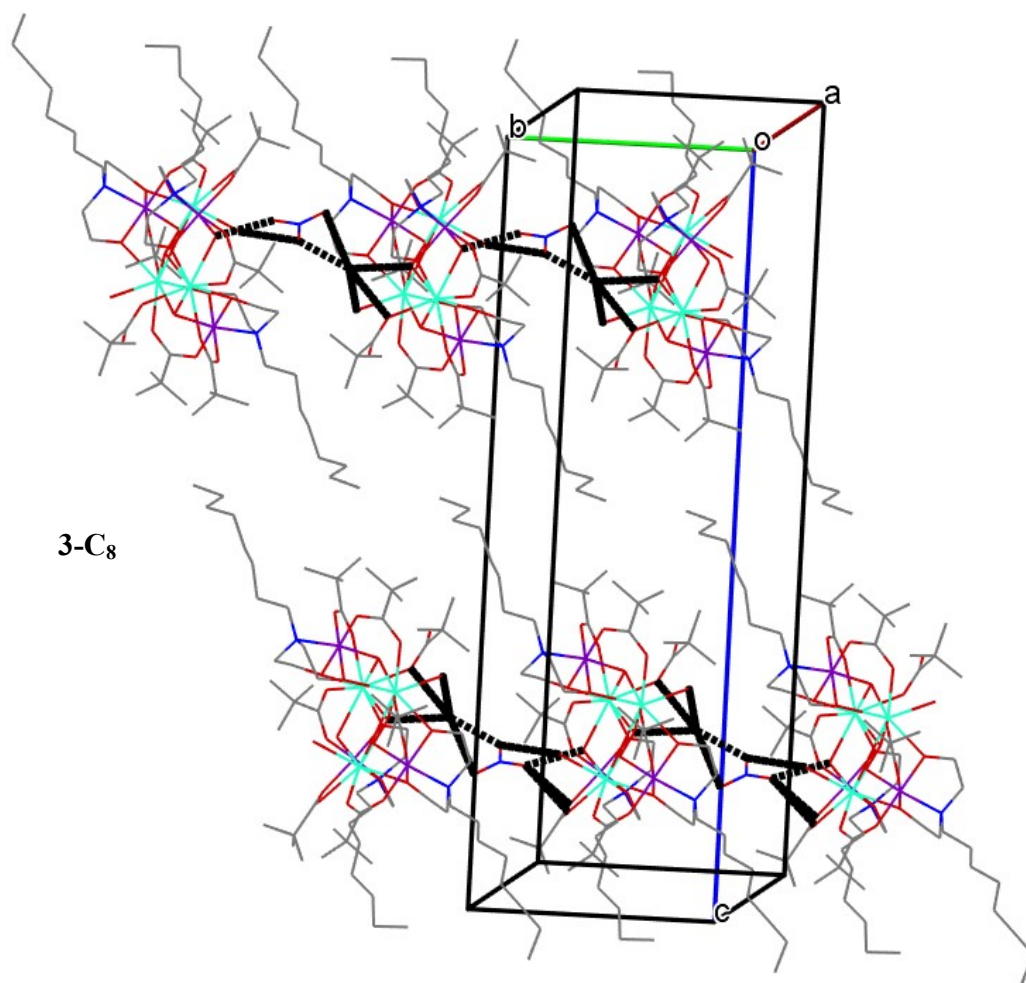


Figure S7. Molecular crystal packing showing the H-bond interaction (black dotted lines) and the C-H...C-H ones (black lines). H atoms omitted for sake of clarity.

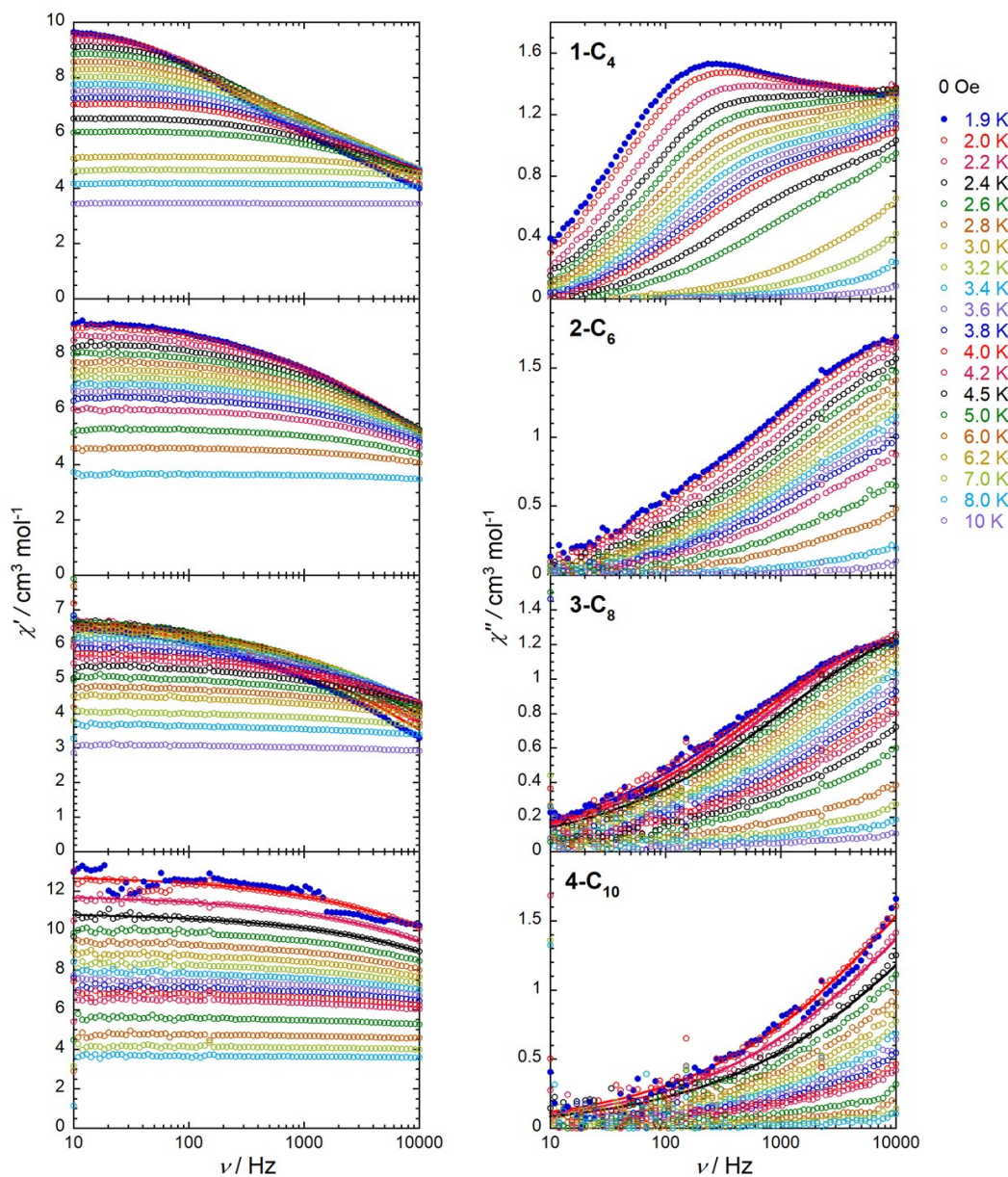


Figure S9: Frequency dependence of the in phase (left; χ') and out of phase (right; χ'') components of the ac susceptibility in zero dc field at indicated temperatures for $1-C_4$, $2-C_6$, $3-C_8$ and $4-C_{10}$. Solid lines are the best fits to a generalized Debye model.

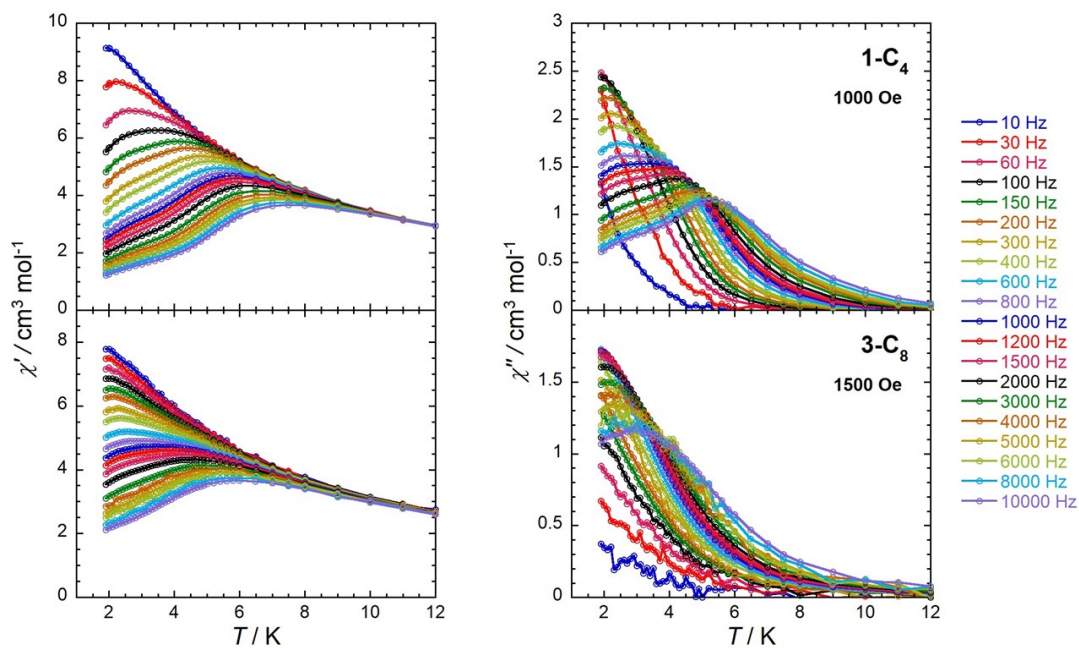


Figure S10: Temperature dependence of the in phase (left; χ') and out of phase (right; χ'') components of the ac susceptibility at optimized dc field and at indicated ac frequencies for **1-C₄** and **3-C₈**. Solid lines are guide for the eyes.

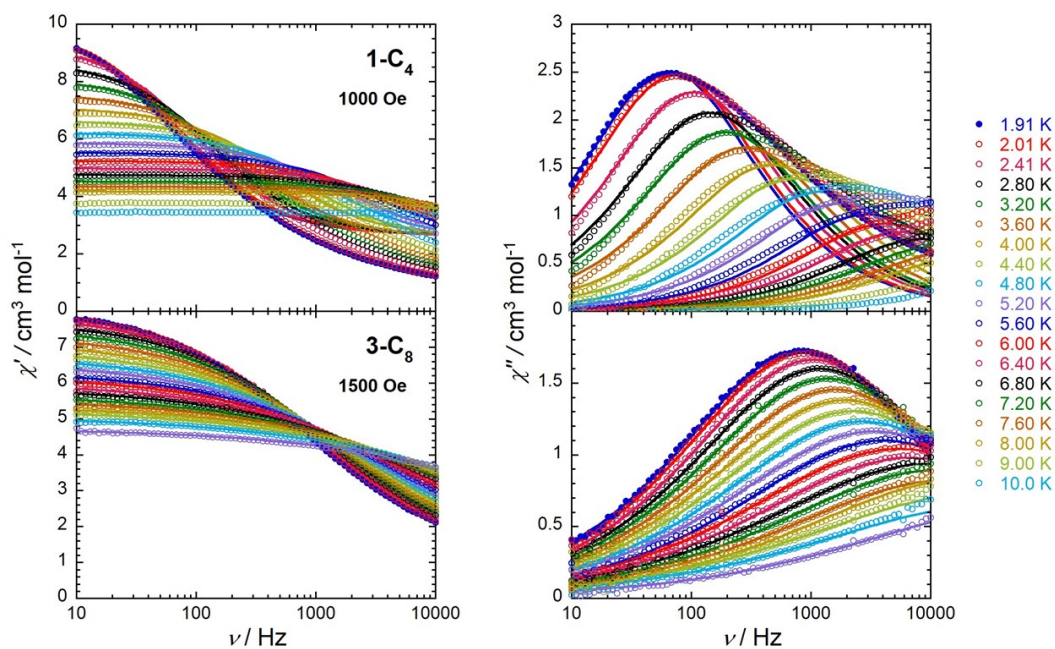


Figure S11: Frequency dependence of the in phase (left; χ') and out of phase (right; χ'') components of the ac susceptibility at optimized dc field and at indicated temperatures for **1-C₄** and **3-C₈**. Solid lines are the best fits to a generalized Debye model.

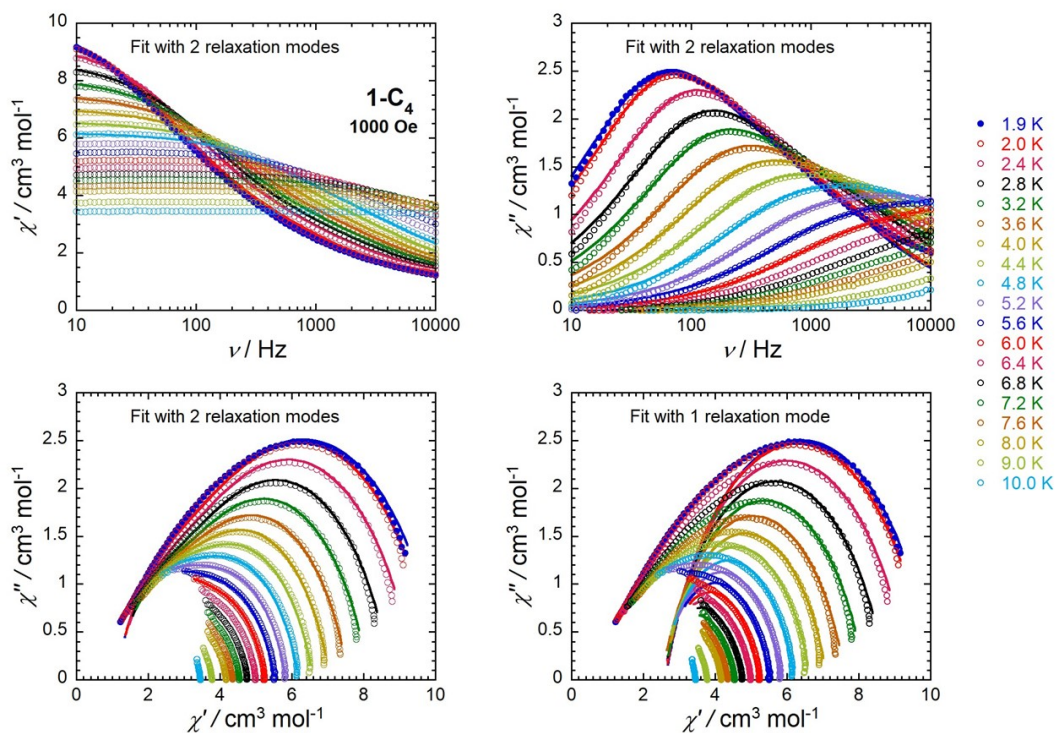


Figure S12: Frequency dependence of the in phase (top left; χ') and out of phase (top right; χ'') components of the ac susceptibility, and the corresponding Cole-Cole plot (bottom left; χ'' vs χ') where solid lines are the best fits to a generalized Debye model considering two relaxation modes. For comparison, corresponding Cole-Cole plot (bottom right; χ'' vs χ') where solid lines are the best fits to a generalized Debye model considering a single relaxation mode. All the data are shown at 1000 Oe and at indicated temperatures for **1-C₄**.

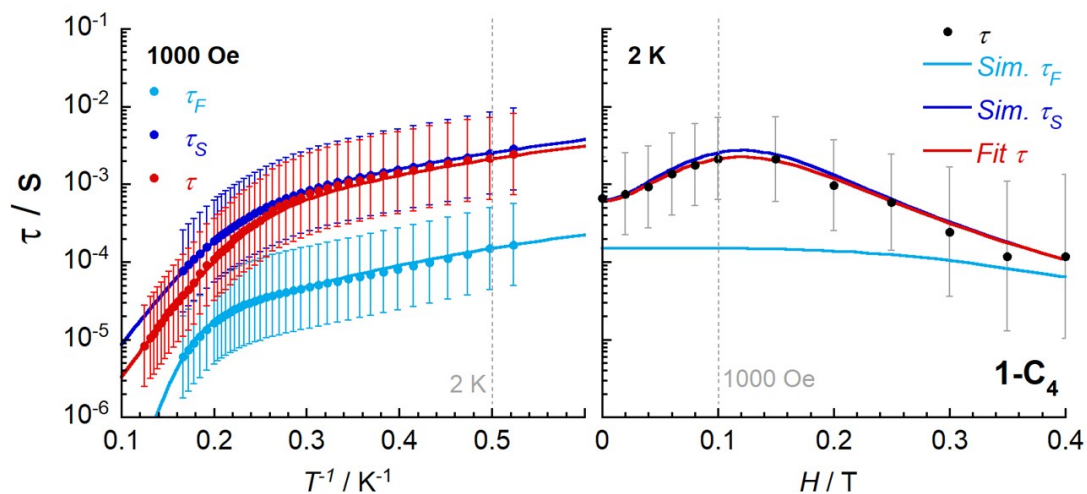


Figure S13: Left: Temperature dependence of the relaxation time (plotted as τ vs T^{-1} in semi-logarith scale) at 1000 Oe for **1-C₄**, considering a unique (red dots; τ) and two relaxation modes (blue and light blue dots; τ_S , τ_F). Solid lines are the best fits to these models as discussed in the main text. Right: Field dependence of the relaxation time (plotted as τ vs H in semi-logarith scale) at 2 K for **1-C₄**, considering a unique relaxation mode (black dots; τ). Solid lines are the best fits to the model considering a unique relaxation mode (red line), and simulations with the model considering two relaxation modes (blue and light blue lines; τ_S , τ_F), as discussed in the main text.